Bull Volcanol (2007) 70:221–244
DOI 10.1007/s00445-007-0133-6

RESEARCH ARTICLE

Volcanic hazards at Mount Semeru, East Java (Indonesia), with emphasis on lahars

Jean-Claude Thouret · Franck Lavigne · Hiroshi Suwa · Bambang Sukatja · Surono

Received: 12 April 2006 / Accepted: 9 March 2007 / Published online: 28 June 2007

Abstract Mt. Semeru, the highest mountain in Java (3,676 m), is one of the few persistently active composite volcanoes on Earth, with a plain supporting about 1 million people. We present the geology of the edifice, review its historical eruptive activity, and assess hazards posed by the current activity, highlighting the lahar threat. The composite andesite cone of Semeru results from the growth of two edifices: the Mahameru 'old' Semeru and the Seloko 'young' Semeru. On the SE flank of the summit cone, a N130-trending scar, branched on the active Jonggring-Seloko vent, is the current pathway for rockslides and pyroclastic flows produced by dome growth. The eruptive activity, recorded since 1818, shows three styles: (1) The persistent vulcanian and phreatomagmatic regime consists of short-lived eruption columns several times a day; (2) increase in activity every 5 to 7 years produces several kilometer-high eruption columns, ballistic bombs and thick tephra fall around the vent, and ash fall 40 km downwind. Dome extrusion in the vent and subsequent collapses produce block-and-ash flows that travel toward the SE as far as 11 km from the summit; and (3) flank lava flows erupted on the lower SE and E flanks in 1895 and in 1941–1942. Pyroclastic flows recur every 5 years on average while large-scale lahars exceeding 5 million m^3 each have occurred at least five times since 1884. Lumajang, a city home to 85,000 people located 35 km E of the summit, was devastated by lahars in 1909. In 2000, the catchment of the Curah Lengkong River on the ESE flank shows an annual sediment yield of 2.7×10^5 m^3 km^{-2} and a denudation rate of 4 10^5 t km^{-2} yr^{-1}, comparable with values reported at other active composite cones in wet environment. Unlike catchments affected by high magnitude eruptions, sediment yield at Mt. Semeru, however, does not decline drastically within the first post-eruption years. This is due to the daily supply of pyroclastic debris shed over the summit cone, which is remobilised by runoff during the rainy season. Three hazard-prone areas are delineated at Mt. Semeru: (1) a triangle-shaped area open toward the SE has been frequently swept by dome-collapse avalanches and pyroclastic flows; (2) the S and SE valleys convey tens of rain-triggered lahars each year within a distance of 20 km toward the ring plain; (3) valleys 25 km S, SE, and the ring plain 35 km E toward Lumajang can be affected by debris avalanches and debris flows if the steep-sided summit cone fails.

Keywords Volcanic hazards · Mount Semeru · Java (Indonesia) · Composite cone · Eruptive activity · Lahar · Sediment yield

Editorial responsibility: H Delgado

J.-C. Thouret (✉)
Département de géologie, Laboratoire Magmas et Volcans UMR 6524 CNRS, OPGC et IRD, université Blaise Pascal,
5 rue Kessler,
63038 Clermont-Ferrand cedex, France
e-mail: thouret@opgc.univ-bpclermont.fr

F. Lavigne
Laboratoire de Géographie physique,
UMR 8591 CNRS et université Paris 1—Sorbonne,
1 place Aristide Briand,
92190 Meudon, France

H. Suwa
Disaster Prevention Research Institute, Kyoto University,
Gokasho Uji, Kyoto 611-0011, Japan

B. Sukatja
Balai Sabo, Sopalan, Maguwoharjo, Depok,
Sleman, Yogyakarta, Java, Indonesia

Surono
Directorate of Volcanology and Geological Hazard Mitigation,
55 Jalan Diponegoro,
Bandung, Java, Indonesia

Introduction

Mt. Semeru (8°06′05″S, 112°55′E), one of the most active volcanoes on Earth, is the highest mountain in Java (3,676 m) and belongs to the Semeru–Tengger volcanic massif (Fig. 1). This area of about 900 km^2 encompasses the Bromo–Tengger, Jambangan and Ajek-Ajek calderas, Mt. Kepolo, and the Mt. Mahameru–Semeru cone complex (Fig. 2), including the currently active Jonggring-Seloko crater, now 400 m across and 200 m deep at 3,444 m asl. The rationale for this research is threefold: Firstly, Semeru's persistent and combined eruptive activity, at least since 1884, is unusual for calc–alkaline composite cones. Understanding how phreatomagmatic, vulcanian, and Strombolian regimes can coexist with lava extrusion at the vent is challenging; Secondly, Semeru is one of the most effective lahar producers on Earth. Although *Sabo* (dams and dikes) constructions have been implemented along the radial drainage network, lahar-related disasters caused >1,000 casualties during the twentieth century alone and severe economic losses on the ring plain; Thirdly, Semeru is a real concern to civil authorities owing to the combination of persistent explosive activity and a dense local population. The ring plain of about 1,790 km^2 is home to 941,000 people (in 1999), supporting a population density of 520 per km^2 in the district of Lumajang including a city of 85,000 (Fig. 2). Another 600,000 people live in or near the city of Malang 45 km WNW of the summit (Fig. 1b). Agriculture is the staple activity in the Lumajang district, followed by plantations, and forestry production.

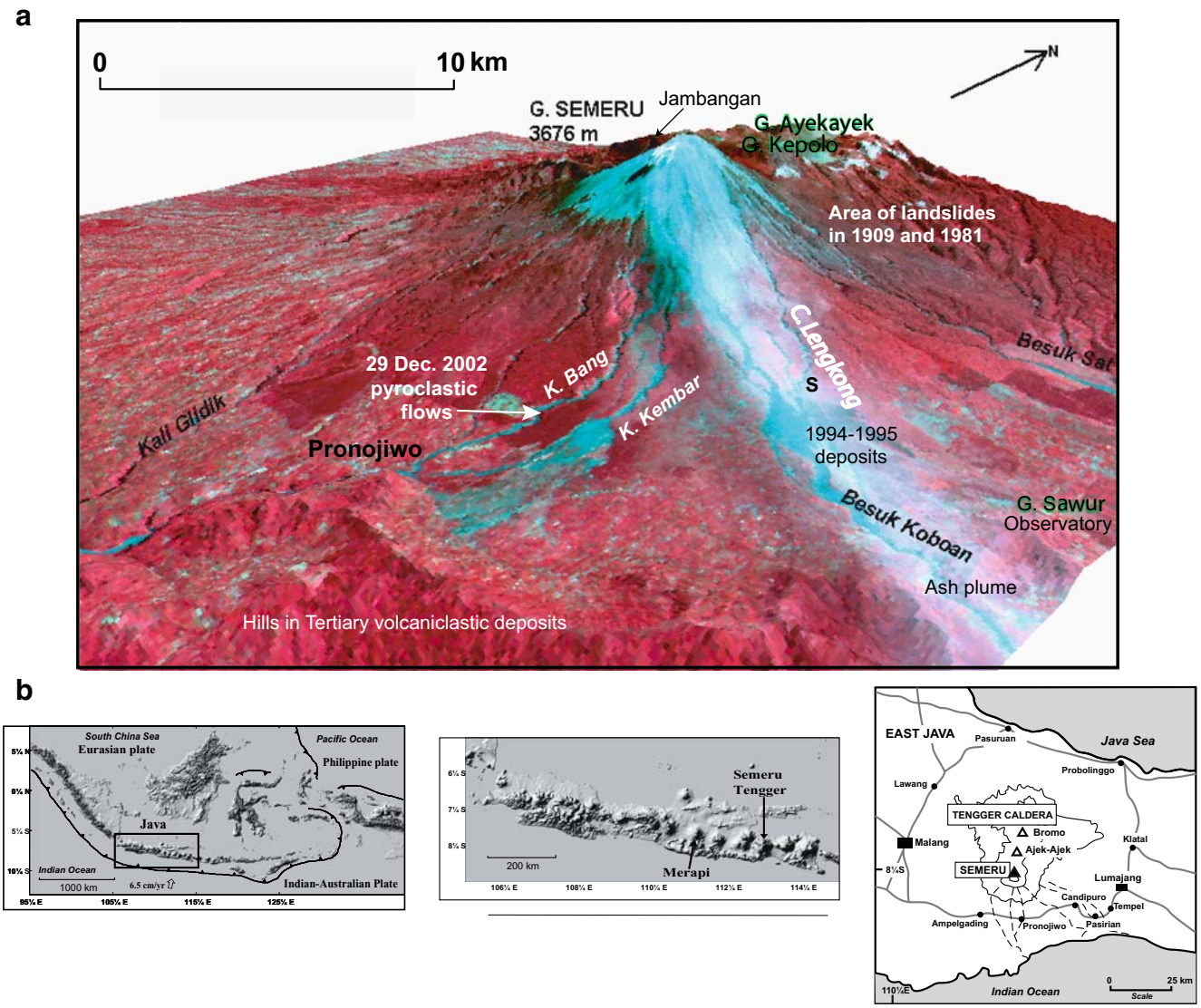

Fig. 1 **a** SPOT satellite image (14 May 1996) draped on a digital elevation model showing the Semeru volcano looking NW. Major rivers and towns are indicated. Valleys affected by most recent lahars and pyroclastic flows in blue. *S* stands for the fixed camera station installed near the confluence of C. Lengkong and Koboan Rivers. **b** Sketch maps showing the geodynamical setting of Indonesia, the island of Java, and the location of the Semeru composite cone in the Semeru–Tengger volcanic massif

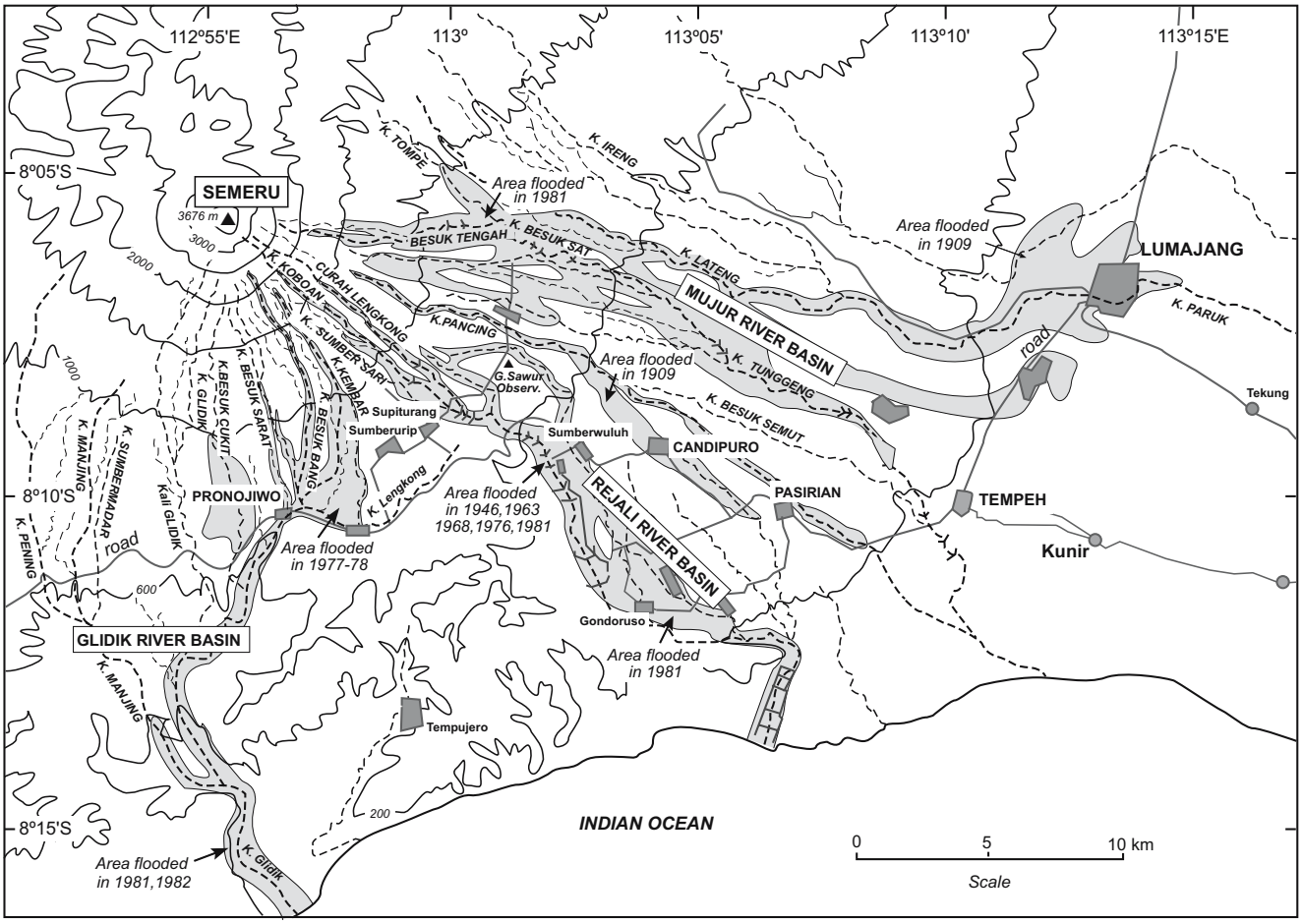

Fig. 2 Map showing the Semeru edifice and the ring plain divided in three Mujur, Rejali and Glidik River catchments. *Grey areas* outline valleys and plains flooded by lahars during the twentieth century. Principal towns and the city of Lumajang are also shown

The goal of this research is to assess hazards and delineate hazard-prone areas based on post-1884 activity and to understand lahars, the most important hazard at Indonesian volcanoes. Firstly, we depict the geology and structural setting of the volcano. Mapping structures and deposits around the heavily forested Semeru draws on high-resolution satellite imagery (Figs. 3 and 4). In addition to a preliminary geological map (1:50,000 scale: Sutawidjaja et al. 1996) and a schematic map of disaster-prone areas (1:50,000 scale: Bronto et al. 1996), our survey is based on three satellite images (multiscanner SPOT4 as of 11 May 1996 and 27 March 2001, and panchromatic SPOT5 as of 24 October 2003). Secondly, we analyse the patterns of Semeru's eruptive behaviour in the light of the post-1884 eruptive activity, products, and aftermath. Unlike Merapi, Semeru has not focused international research but Dutch and Indonesian geologists of the Directorate of Volcanology and Geological Hazard Mitigation (DVGHM, former Volcanological Survey of Indonesia) have provided a wealth of reports describing its activity since 1818. Thirdly, we emphasise the major threat on the ring plain by studying the extent, deposits, and hydraulic parameters of lahars using grain-size and componentry analysis and video camera footage. Finally, we assess volcanic and lahar hazards and we delineate a hazard-prone map that may help to revise the current map of disaster-prone areas (Bronto et al. 1996).

Geological setting

The Semeru–Tengger volcanic massif comprises a cluster of calderas and stratocones developed over a deeply eroded Tertiary volcanic arc in South Java (Figs. 1 and 3; Van Bemmelen 1949; Situmorang 1989; Sutawidjaja et al. 1996). The 8-km diameter Bromo–Tengger caldera formed during the Late Pleistocene (>45 ka and ca. 33 ka: Mulyadi 1992); resurgent volcanism has constructed four stratocones, including the active Bromo tuff cone. S of Tengger, the older nested Jambangan and Ajek-Ajek calderas, open to the E, are thought to have produced debris avalanches (Carn 1999). Near the S rim of the Jambangan caldera, the Holocene G. Kepolo stratocone is lined up with a youthful

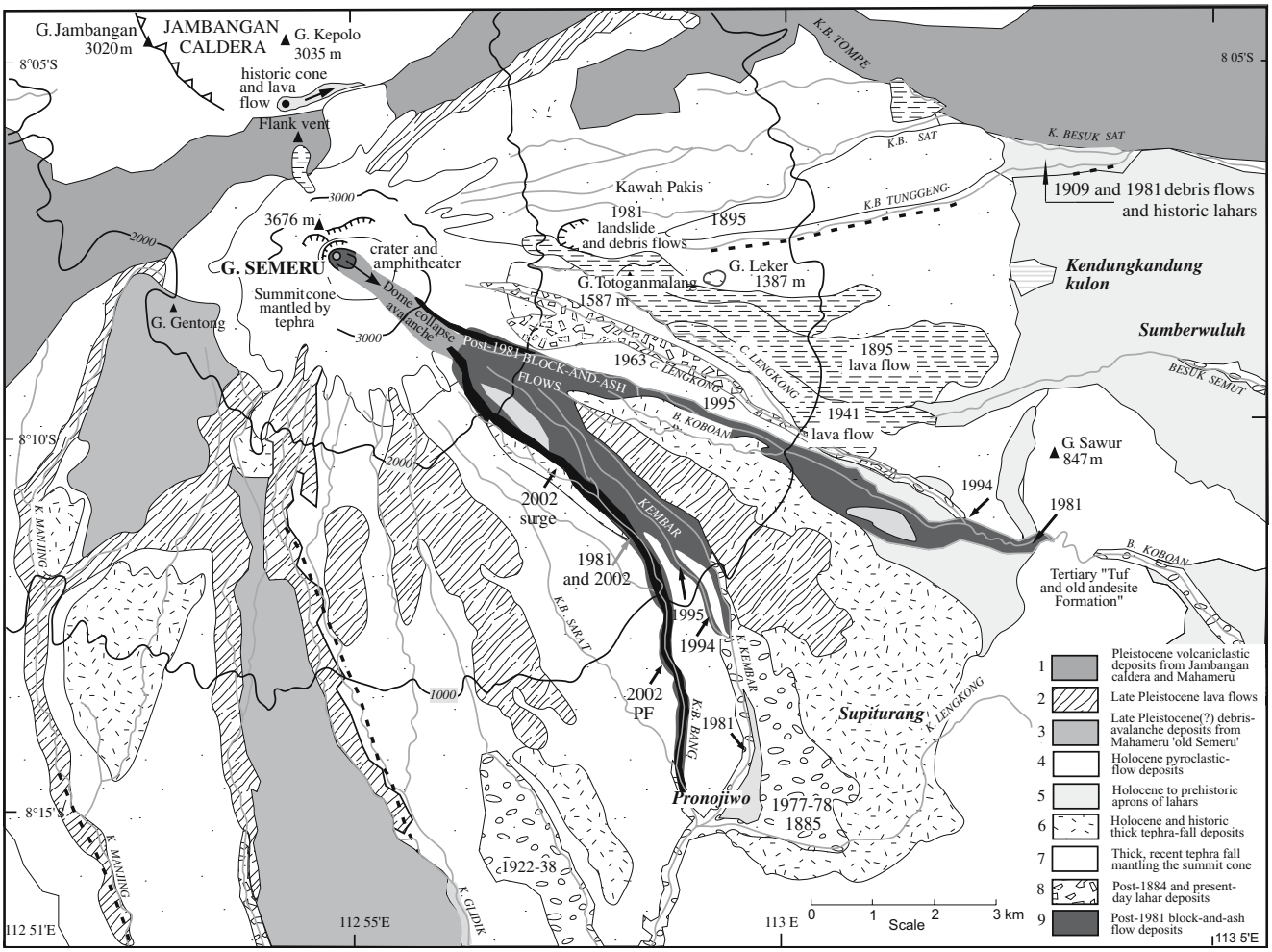

Fig. 3 Geological map of the Semeru composite cone and ring plain (based on Situmorang 1989; Simkin and Siebert 1994; Wahyudin 1991; VSI geological map by Sutawidjaja et al. 1996; Siswowidjoyo et al. 1997; Carn 1999; aerial photographs 1990–1991, and three SPOT 4 and 5 scenes at 20 m and 2.5 m resolution). Stratigraphic units 1 to 9 keyed to symbols in map. The extent of the 29 December 2002 pyroclastic flow and surge in the K. Bang valley is outlined as well as the scar of the 1981 landslides on the E flanks of Semeru. White areas of the map are Tertiary rocks of the 'Tuf and old andesite Formation' to the SE, and Tertiary and Quaternary volcanic rocks of the Jambangan massif and caldera to the NW

lava cone and flow at the foot of the N Semeru's flank. Semeru, including the currently active Jonggring-Seloko vent, is superimposed on, and buttressed to the N, by the Jambangan complex. To the S and SE, Semeru overlies weathered tuffs and breccias, and lava flows of the Oligocene–Miocene 'Tuf and Old Andesite formation' (Figs. 2 and 3).

Semeru composite cone

A geological sketch map (Fig. 3), based on a 1996 SPOT4 image, on field surveys, and on the geological map by Sutawidjaja et al. (1996), displays the cone-shaped summit of Mt. Semeru covered by thick tephra above 800 m asl, volcaniclastic fans between 800 and 400 m asl., and the ring plain below 400 m asl. Overlying the voluminous Late Pleistocene 'old' Semeru (=Mahameru) stratovolcano, the bulk of the 'young' Semeru cone (about 60 km^3 of mafic medium-K andesites 55–57 wt% SiO_2) may be Holocene in age (Sutawidjaja et al. 1996). Three structural features are inferred from a digital elevation model (DEM; Fig. 4a, 30m resolution), computed on digitised topographical maps

Fig. 4 **a** DEM based on digitised topographic maps (1:25,000 scale) and draped with a SPOT5 scene (2.5 m pixel), looking NE. A structural boundary no. *1* is indicated between the two edifices (*M* Mahameru or 'old' Semeru; *JS* Jonggring–Seloko of 'young' Semeru), which have formed the Semeru composite cone; no. *2* indicates the 1.5-km long × 0.35 km wide horseshoed-shaped scar, SE of the active Jonggring–Seloko vent (no. *3*), that guides rockfall, avalanches, and pyroclastic flows. Note quasi-circular fissures suggesting deformation by lava extrusion around the vent area. Landsliding area on the E flank and gullies that conveyed landslide-triggered debris flows in 1909 and 1981 are also shown. **b** Aerial photograph (1991: Perum Survey Nasional—flight 1982 RS-N9, courtesy: Mt. Semeru Project) showing the inferred structural boundary between 'old' and 'young' Semeru and the rims of three vents nearby the Mahameru summit that preceded the active Jonggring-Seloko vent and scar open toward the SE

(1:25,000 scale) and draped by the 2003 SPOT5 scene (2.5-m pixel), and from the 1990 aerial photograph (Fig. 4b): (1) A structural boundary is drawn between the 'old' and 'young' Semeru cones. The western branch of the large-angle scarp parallels the N80-trending strike-slip fault (Fig. 3) while the eastern branch coincides with a N105-trending Riedel fault (i.e. the S lip of deep-seated landslides on the E flank); (2) Three arcuate scarps in the summit area suggest that vents have migrated from NW to SE, from 'old' to 'young' Semeru, i.e. toward the Jonggring-Seloko vent, which reportedly

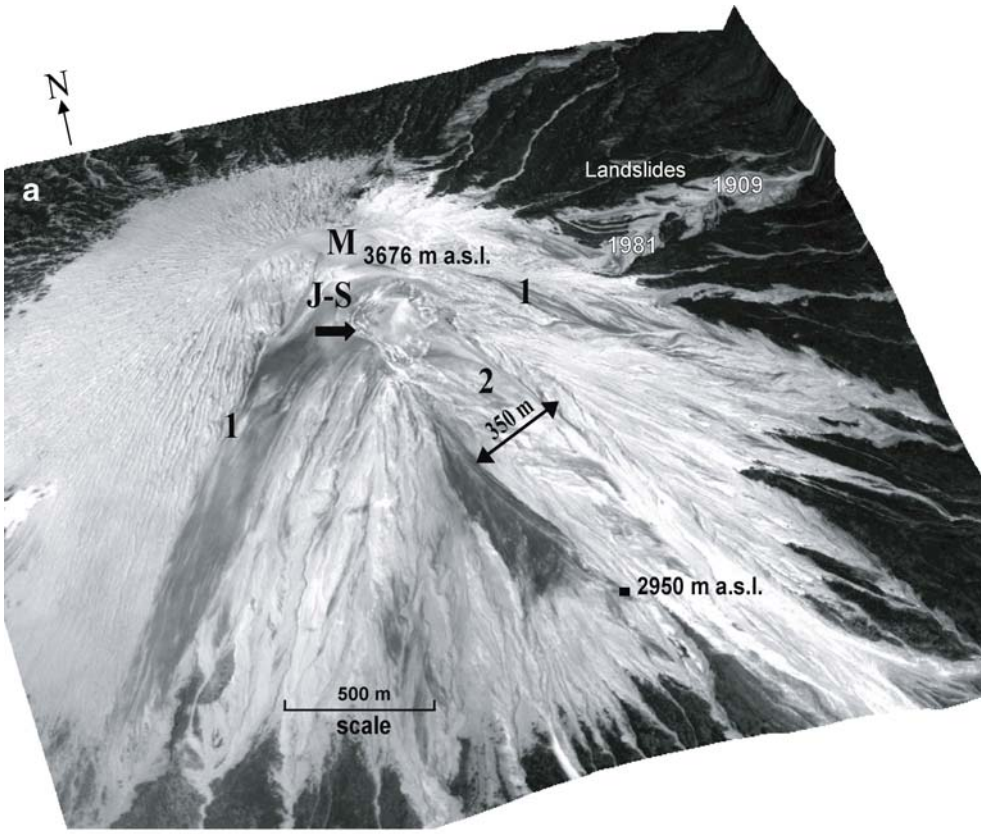

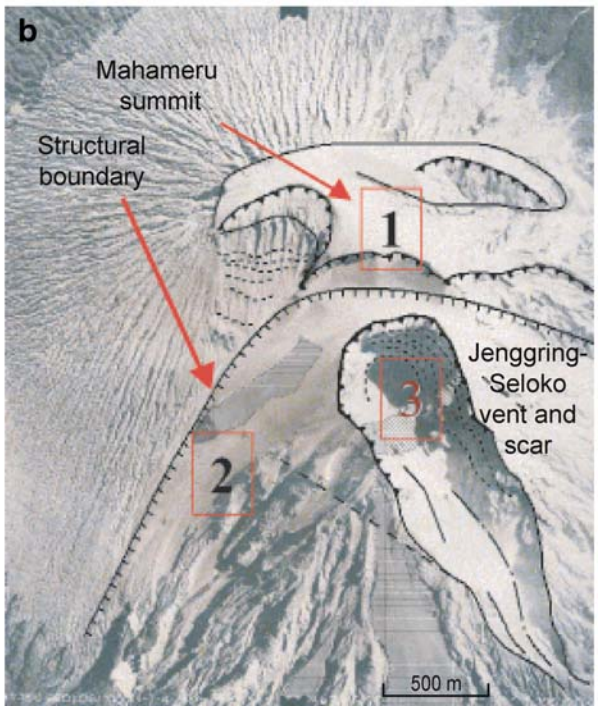

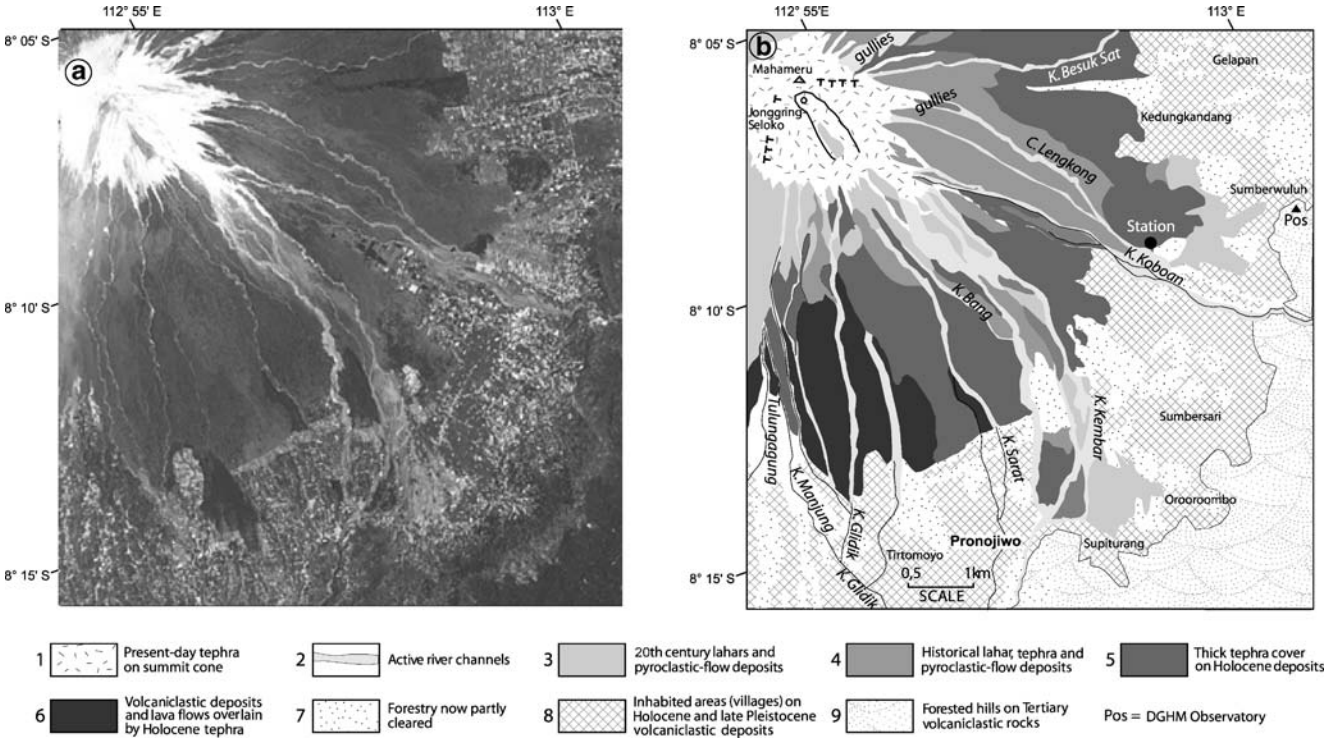

Fig. 5 **a** Extract of the 23 October 2005 SPOT5 image (2.5 m pixel) interpreted in **b** a geological sketch map of deposits on the SE flank swept by the Holocene and present-day pyroclastic flows and debris flows. *Key: 1* Present-day tephra on summit cone; *2* channelled present lahar and pyroclastic-flow deposits in gullies and narrow valleys; 3 unchannelled and bare tephra-fall and pyroclastic-flow deposits on the composite cone; *4* historical tephra-fall, lahar, and pyroclastic-flow deposits; *5* thick tephra cover on Holocene deposits; *6* volcaniclastic deposits and lava flows overlain by Holocene tephra; *7* volcaniclastic deposits and lava flows covered by forests (now mostly cleared); *8* inhabited areas and villages on Holocene and older volcaniclastic deposits; *9* forested hills on Tertiary volcaniclastic rocks termed 'old tuff and andesite formation'

initiated in 1913 (Van Padang 1951; Siswowidjoyo et al. 1997); (3) Breaching the active vent, the NW–SE-trending horseshoe-shaped scar cuts down >1 km long and 0.35 km across the steep-sided SE flank.

The DEM looking NW (Fig. 4a) shows the horseshoe-shaped scar that now guides pyroclastic flows and rock-slides toward the K. Kembar and K. Koboan catchments. Historic lithographs (Dana 1997) suggest that the scar may have been alternatively filled by summit lava flows and cut down again and, subsequently, may have migrated on the SE flank. That scar was drawn along the K. Besuk Semut in 1963 but it branches out in the three K. Bang, Kembar, and Koboan valleys in 1994 (Fig. 2). The DEM also highlights landslide scars on the E flank and gullies farther downvalley in Besuk Tengah, Sat, and Tunggeng Rivers (Fig. 2), which have supplied material to debris flows (≥6 million m^3) in 1909 and 1981 (Siswowidjoyo et al. 1997).

In addition to historical lava flows, the volcaniclastic fans of the ring plain comprise debris–avalanche deposits (of Mahameru?) toward the S and SSW, Holocene to historical pyroclastic flow deposits of 'young' Semeru, present-day lahars, and a tephra cover (Fig. 3). Situmorang (1989) outlined ten units produced by the Mahameru–Semeru volcano forming ten fans on the basis of the radial network of rivers that drain the SW, S and E flanks of the cone. The 2003 SPOT5 image allows us to accurately outline deposits on the S and SE flanks that are often affected by pyroclastic flows and debris flows since 1967, i.e. from the K. Glidik valley to the Besuk Sat valley (Fig. 5a–b). The extensive Semeru ring plain can be divided in two ways. Firstly, 'old' fans of volcaniclastic material prior to Holocene, which are not inundated by lahars at present, are distinguished from the flood-prone 'young' ring plain, which is made up of Late Holocene and pre-1800s deposits. The most recent deposits form low terraces that have been flooded during large events since the 1800s (e.g. Fig. 2). Deposits of lahars laid down since the 1980s appear bare and dark (=water saturated) on satellite scenes (Fig. 5). Secondly, three major drainage systems are outlined (Fig. 2): the Glidik River and tributaries convey lahars 20 km S to the sea, the Rejali River and tributaries more often carry lahars SSE to the sea 25 km; the longer, denser, braided network with gentle slopes (1.3%) of the Mujur River have conveyed more voluminous, albeit less

Table 1 Semeru eruptive behaviour displays three coexisting eruptive styles

Reported date	Valley, flank, direction and distance	Victims; Damage (D)	Event and deposits*	Observed activity, magnitude, and aftermath
Period 1884–1963				
10–11 December 1884 to 14–18 April; 4, 7 September 1885	Koboan, SE, Besuk Semut, Kembar, Bang, Sarat	70 to 85; 2 villages, plantation	Lf, Tf, Pf, syneruptive *Lh*	Expl. preceded by a 26 10^6 m^3 landslide of crater rim and lava tongue, April 1885
January 1886, August 1887	Vent area		Tf, Lf**	Expl.; flank Lf*? = extrusion and rockfall?
February–October 1888	Vent area		Tf, Lf**	Expl.; avalanches?
January 1889–May 1891	Vent area		Tf, Lf**	Expl.; flank Lf*? = extrusion and rockfall?
1892–1893	Vent area		Tf	Expl.
22–23 May–10 July, 1 October 1895	Besuk Sat, Tunggeng, Pancing E; Lengkong SE	80(?) Devastated arable land	Tf, Lf*; *Lh*	Expl., flank Lf: several 10^6 m^3, reported 'overflow'
May–June 1896	Vent area, Tunggeng		Tf, *lh*	Explosions
January 1897, February 1898	Vent area		Tf, Lf*	Expl.; lava extrusion and rockfall?
January, March, Dec. 1899	Vent area		Tf	Expl.
29 March–11 April 1900	Vent area		Tf, Lf*	Expl.; (flank?) Lf*=extrusion and rockfall?
1901–1905, 1907, Nov. 1908	Vent area		Tf, *Lh*	Explosions
22 March 1909: most severe lahars (—Sept 1910)	Besuk Sat, Tunggeng, Lateng, East flank, 35 km	220 Victims, 38 villages, cattle; 1450 houses in Lumajang; 110 km^2 flooded land	Landslides and *Df*	Overflow K. Sat–Tunggeng to K. Pakel–Lateng
January–February, 16 November 1911, 28 August 1912	Vent area, scar, flank? Glidik	Devastated arable land	Tf, Pf, Lf*, *L*h	Expl.; flank Lf? Synerup–tiveLh in K. Glidik
23–26 June 1913	Vent area; Besuk Semut E	Devastated arable land	Tf, Lf*, *Lh*	Expl.
1914 (1916)	Koboan, Rejali, SE	Devastated arable land	*Hot Lh*	
21 September 1941–February 1942	Besuk Semut, C. Lengkong, SE, 6.5-km long lava flow ESE	Devastated arable land and irrigation	Lf 6.5 km long (1,470–765 m asl); Lf, Tf	NW–SE fissure 1.3 km long (1,775 to 1,400 m asl), vol. 3 10^6 m^3 (1 month)
12–18 June 1945	Vent area			Expl.
February–May, October – December 1946	Summit area and scar toward SE?	Fatalities; devastated arable land, Sumberwuluh	Tf, Pf, hot Lh	Expl.; do. gr. and Aval;
March–June 1947	Vent area	Damage	Tf, Pf, *Lh*	Expl., do. gr.
1948	Koboan, Rejali, SE	Damage	Lh	Overbank in Sumberwuluh
23 July, 28 August, November–December 1950	Vent area; Besuk Sat; Besuk Semut	Damage	Tf, Pf, *Lh*	Expl.; do. gr., coll. And 'Lf': probably avalanche
November 1951; 1952	Vent area; Semut, Koboan, Lengkong, E, SE		Aval., *Lh*	Do. gr.
November 1954	Summit vent and scar; towards SE		Tf, Aval.	Expl., do. gr.

Table 1 (continued)

Reported date	Valley, flank, direction and distance	Victims; Damage (D)	Event and deposits*	Observed activity, magnitude, and aftermath
1955–1957 (February 22, May 4)	Lengkong, Rejali, SE; K. Sat, Tunggeng, Lateng, E	220 Victims; damage	Aval., *Df*	Do. gr.; landslides on E flank; Dfs and flood reached Lumajang
1958–1960 (April–May, August)	Vent area, Glidik 1 km; Lengkong, Semut		Aval., *Lh*	Do. gr.
1961	Vent area; Glidik, Sarat, Koboan, S, SE		Fountaining? 3-km high ash column above vent; Aval.	Violent "Strombolian"-type eruptions
1963–1964 5 May 1963	Koboan, Lengkong SE; Besuk Semeut, Pancing E, 8 km	? victims Damage	Tf, Aval., Pf, *Lh*	"Strombolian"-type eruptions, 3,000-m high ash column above vent
Period 1967 (onset of persistent, 'mixed' vulcanian activity and dome growth)—2003				
31 August–September 1967	Summit vent and scar, SE 7 km? Koboan, Rejali, Lipark	Damage in villages, Sumberwungkal	Tf, Aval., *Lh*	Expl., do. gr. and coll.
9 March 1968	Glidik, Koboan, Rejali, Liprak SE; 1.5 et 4.5 km	5 Victims, damage: Sumberwungkal, arable land	*Lh,* floods; Aval. 1.5 km?	Avulsion from Rejali to Liprak at 500 m asl
1969	Vent area SE, 1.5 km		*Lh*	Do. gr., Aval.
1972	Glidik, S	No victim? Devastated forest	Aval., Pf	Explosive activity (column 0.5 km high) and do. gr. 3744.5 m
1973	Besuk Sat, Koboan, 2 km	Devastated forests	'Lf' fountain	Do. gr. and Aval.
1974, 22 August	Vent and scar; Liprak, Regoyo, Rejali, Kembar, Bang	Damage: Sumberwungkal and other villages	Tf, Aval., *Lh* 3.84 10^6 m^3	Expl., do. gr.
April, 22 July 1975	Vent area; Tretes, Kembar,	Damage to several villages, arable land	Aval., Pf, *post-event Lh*	Do. coll.; Aval. 5.4 10^6 m^3
16 September 1976	Koboan, Liprak, Rejali SE, 1.7–2.6 km			
13 November 1976	Glidik, Lengkong, Koboan, Rejali, Liprak, Mujur SE, Kembar, Bang SSE	133 Victims; cattle, devastated villages: Renteng, Kebondeli, Sumberwungkal, 335 ha arable land, roads	*Large Lh* ca. 4.65 10^6 m^3	Avulsion and floods
1st December 1977				
14, 16, 23 December 1977	vent and scar, Kembar, SE 10 km, 780 m asl Kembar, Lengkong	No victim? Several villages, pine forest, and arable land devastated	Aval., Tf, Pf, *large Lh*	Do. Lava tongue coll. 6.4 10^6 m^3
January June, 20 September 1978	Glidik S; Kembar, Koboan, Liprak, Lengkong SE, Lengkong SSE	12 Victims; damage to main road Dampit–Lumajang, 125 ha rice and pine, villages (Sumberurip), roads	Tf, Aval., *Lh*	Expl., do. gr.; temporary lake near Sumberurip
1980	Besuk Sat, Koboan, Bang, Kembar, Glidik S, 7 km?		Aval.	Explosive activity, Do. gr.
28, 29, 30 March, 3, 5 April 1981	C.Lengkong, Kembar, Bang, SE 10 km; Glidik, S, 7 to 11 km,	252 victims, 152 wounded 365 victims. Widespread	PFs, *hot Lh,* Aval., Df *Hot Lh*, overbank	Do. coll. 6.2 10^6 m^3 Landslide on E flank (1,600–2,000 m asl), 6.0 10^6 m^3
14 May 1981	Besuk Sat, Tengga, Tunggeng, Mujur, E, 30 km	Damage: 918 ha rice, 16 devastated villages, evacuation		
May 1982–16	C. Lengkong, Kembar,	No victim? Damage to	*Lh, Pf*, Aval.	Several villages

Table 1 (continued)

Reported date	Valley, flank, direction and distance	Victims; Damage (D)	Event and deposits*	Observed activity, magnitude, and aftermath
January 1983	Koboan, SE, 3.5–4 km; Glidik, S, 7.5 km	villages		relocated before *Lh* flowed down to S, 6 10^6 m^3
10 May 1985 15–18 August 1985	Vent area (collapse), Tretes, Koboan, Kembar SE 5 km. *Unusual lahars in dry season*	70? (Front near Pronojiwo) *Damage* to Jugosari village, Liprak	Tf, Aval., Pf? *Lh*	Expl., 1-km high columns, do. coll.; Pf deposit 5 10^6 m^3
1986 July 1987	Rejali, Tretes, Koboan, C. Lengkong, SE, 5 km		*Lh, Tf, Aval.*	D. to villages, arable land Expl., do. gr.
10 May 1988	Kembar, Tretes, Koboan, C. Lengkong; SE, 7 km		Tf, Pf, Aval.	Expl., do gr, 5 10^6 m^3
21 December 1990	Jonggring–Seloko vent Kembar, Koboan		Fire fountain Aval.	"Strombolian" expl., coll. of the crater floor?
1991	Scar, Kembar, SSE, 0.5 km		Aval.	Lava extrusion
1992	Vent area	3 Victims; damage to arable Land and houses	Tf	Expl., 1-km high column
3 February 1994	Scar, Koboan, Lengkong; 11.5 km; Kembar SSE, 7.5 km (750 m asl)	8 Victims, 275 evacuated; Sumbersari covered; 1.5 km^2 plantation, Oroombo and Renteng devastated	Bl-a-a-Fs 6.3. 10^6 m^3, Ps, Tf; *post-event Lh*	Do. coll. and ash-cloud Ps
20 July 1995	Kembar, Koboan, C. Lengkong, SE 7.5–11.5 km (840 m asl)	Several villages evacuated, arable land devastated	Bl-a-a-Fs 5.5 . 10^6 m^3 *post- event Lh*	Do. coll.
August–September 1996	Kembar, SSE, 2 km		Tf; Aval.	Do.gr. and coll., Pf., high columns
July–November 1997	Vent area, scar SE, 2 km; C. Lengkong	2 Tourists on 2 September 1997	Ballistics; Tf dispersed 46×18.5 km to the WNW	Expl.: 3.7–4.9-km high columns
March–Sept 1999	Vent area, scar, Kembar, SSE, 2 km		Aval.	Expl.; do. gr.; 9-km high columns
May–July, December 2000	Vent area, Kembar, Koboan, SE & SSE, 3 km	2 Volcanologists killed and 5 wounded, 27 July 2000	Tf 11 km; Pf	Expl., do. Gr.; high columns
2001–2002	Vent and scar, Kembar, 0.75–2.5 km		Tf; Aval.	High columns in June–September
23–29, 30 December 2002	Vent area and scar; Bang, SSE, 9 km Supit near Pronojiwo, 750 m asl; Kembar, SSE, 1.5–4 km, avalanches	No victim; damage on forest by ash-cloud surge; Supit (Pronojiwo) evacuated	Bl-a-a-F and wet Ps: 3.5. 10^6 m^3 and *hot Lh* in K. Bang on 29 December 2002; Tf 12 km; *Lh*	Activity increased since March 2002 (Alert level 2). Expl., high columns; do. coll.;
March–May 2003	Vent area and scar; Bang and Kembar SSE, 1.5–3.75 km		Aval.; Pf, Lh	Explosive activity; do. gr. and do. coll.; alert level 2, MODIS thermal alert

Semeru eruptive behaviour since 1884 (Kemmerling 1922; Van Bemmelen 1942; Kusumadinata 1979; GVN 1996, 1997, 1999, 2000, 2001, 2002, 2003). All eruptions ranked VEI 2 by Simkin and Siebert (1994) except VEI 3-ranked and (or) damaging events in bold.

Lh Lahars (large volume: Lh in italics); *Df* debris flow; *Lf* lava flow; Lava flow* reported before 1950, interpreted as extruding lava that collapses from the vent into the active scar on the SE flank. *Tf* tephra fall; *Pf* pyroclastic flow; *Bl-a-a-F* block-and-ash flow; *Ps* pyroclastic surge; *Aval.* rockslide avalanche from lava extrusion or dome; *Expl.* explosions; *do. gr.* dome growth; *do. coll.* dome collapse

frequent, debris flows 35 km to the E beyond the city of Lumajang in 1909. Debris-flow deposits in the Besuk Sat, Tengah, and Tunggeng valleys that drain the E Semeru's flank witness to the 1909 and 1981 landslide-induced debris flows. Unvegetated deposits with undulated levees and channels on the SPOT scenes form an irregular triangle area between the upper K. Tunggeng and Besuk Sat–Tompe valleys (Figs. 2 and 5). On the SE flank, an

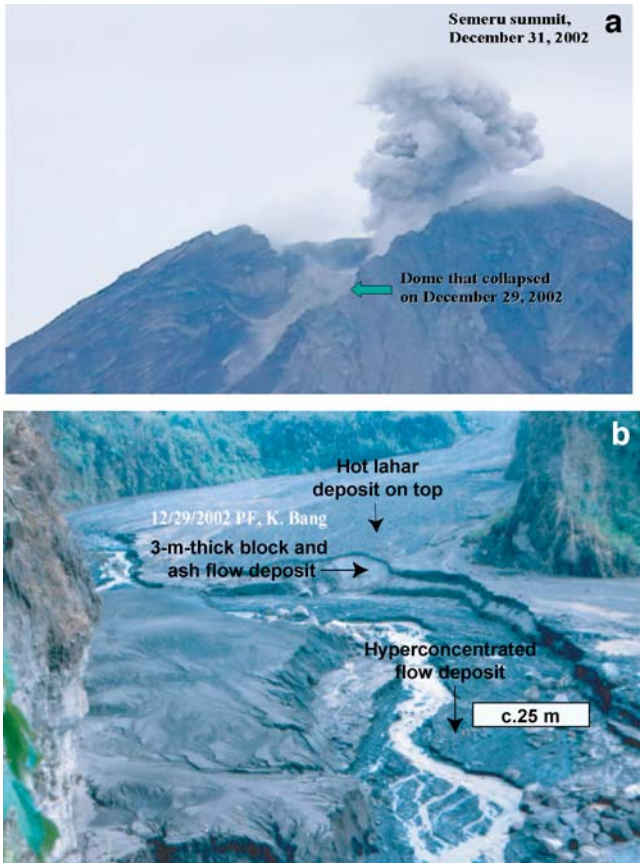

Fig. 6 **a** Photograph (JCT) looking NNW toward the vent and remnant of a dome in the active scar at the top of the SE flank, taken the day after the 29 December 2002 dome collapse-induced pyroclastic flow was channelled in the K. Bang valley. **b** Photograph (JCT) taken on 31 December 2002 at Supit (Pronojiwo) showing the distal part of the 29 December 2002 block-and-ash flow deposit 2 m thick in the K. Bang valley 11 km of the summit. Dark hot lahar deposit overlays the whitish block-and-ash flow deposit while the active channel remobilises thin hyperconcentrated flow deposits

area having a dark spectral signature forms an apron of pyroclastic flow and lahar deposits between the K. Bang and Kembar valleys and the C. Lengkong and K. Koboan valleys. Thick lahar deposits and alluvium have ponded against the scarps of the southern hills and have choked the gorges that cut down their weathered volcanic rocks (e.g. K. Koboan–K. Sumbersari between Supiturang and G. Sawur).

Post-1884 patterns of eruptive activity

Very little is known about the pre-historic activity of Semeru as scientific reports extend back to 1884 only, although activity was reported as early as 1818. Unrest has been continuous since 1967 (Simkin and Siebert 1994; Wahyudin 1991). Based on many reports that describe height, colour and direction of ash and gas columns, flank and summit eruptions, and extent of pyroclastic density currents (Table 1), the persistent Semeru eruptive behaviour displays three coexisting eruptive styles, which challenge our understanding of eruption behaviour and magma output rate.

Considered to be the background explosive activity, the first eruption style is threefold: (1) short-lived whitish to grey gas-driven columns rise 300–1,000 m above the crater at intervals of 5 to 40 min several times a day and are followed by rapidly declining ash emission. They result from phreatic or steam explosions (of rain ponding on crater floor) that commence with degassing and the sound of breaking rocks and are followed by a shower of lithic ash and blocks without juvenile material; (2) "cannon-like" explosions trigger 1- to 3-km high vulcanian columns that disperse ash >25 km toward the E, SE, W–SW, and occasionally to the N; (3) phreatomagmatic explosions expel small volumes of non-juvenile dense lava fragments and bread-crust bombs, which are occasionally hurled >0.5 km beyond the rim; vulcanian and(or) phreatomagmatic explosions, producing dark and sometimes cock-tailed, ash-laden high columns, reflect magma–water interaction at the vent floor, described as wet by observers at the Mahameru summit (GVN 1997): bread-crust bombs in ejecta also indicate surficial water–magma interactions. The first three regimes aforementioned coexist with relatively slow rates of lava extruding from a dome plug as shown by the 26 September 2004 SPOT5 scene (NUS-CRISP 2006), which produces incandescent rockfall avalanches that typically reach 0.5 to 1.5 km along the SE scar. Vesiculated lava and lighter (2.60 g cm^3) scoriaceous blocks of mafic andesite (55–56 SiO_2 %), dragged from the extruding lava, imply degassing processes involving magmatic gas interacting with an aquifer at the conduit-vent host rock boundary (GVN 1996, 1997). This interaction can explain three observations: short-lived, little ash-laden vulcanian columns that propel bread-crust bombs, incandescent blocks stripped off the extruding lava at the vent bottom, and light porous lava of the dome plug.

In contrast, the second eruptive style is linked to accelerated extrusion rates every 5 to 7 years. Increase in output rate of more volatile-rich magma triggers: (1) 3- to 7-km high columns producing ballistic bombs to 1.5–3 km and ash fall 35–45 km downwind; and (2) block-and-ash flows, induced by dome collapse sweep the SE scar and channelled 5 to 12 km downstream K. Bang, Kembar, and Koboan valleys at a about 5-year interval (e.g. 1972, 1977, 1981, 1994, 1995, and 2002). The 3 February 1994 pyroclastic flows with a volume of 6.8×10^6 m^3 swept the K. Koboan and Lengkong valleys as far as 11.5 km from the vent on the SE flank (Sadjiman et al. 1995; Table 1). On 20 July 1995,

Table 2 Frequency, magnitude, travel distance and other parameters for hazardous events (lahars) at Semeru based on reports or records since 1885

Occurrence and intensity	Average discharge	Volume (10^6 m^3)	Deposit thickness	Travel distance	Observations
Rainfall season (Oct.–May)	250–300 m^3 s^{-1} every year	Small: <0.1–0.5 several per year, daily during rain season	Min. 0.25–0.80 m, max. 4–6 m; average 1–2 m; beds succession during long-lasting (3 h) events up to 6 m	Maximum debris flows	*Largest lahars* induced by landslides and heavy rainfall (e.g. 1909, 1981)
Average 50–120 mm/day and 200–350 mm/month (May 1946, June 1956)	500–600 m^3 s^{-1} every 5 years	Average 1.5 (2 per year)		>35 km (1909: Lumajang, Fig. 1); average 15–20 km	*Large syneruptive hot lahars* at least 7 times since 1885
Max.:315–390 mm/day and 182 mm/hour (14 May 1981)	800 m^3 s^{-1} every 10–20 years	1.5 <large volume <6.0		Hyperconcentrated flows travel shorter distances	*Large post-eruptive* lahars: every 5.5 years
400–750 mm/month (1550 mm, (March 1957, June1960)	Maximum 2,200 m^3 s^{-1} in March 1981 (Tung-geng: Mt. Semeru Proyek)	Every 6 years since 1885			

pyroclastic flows traveled 9.5 km downstream the Koboan valley (Dana et al. 1996; Fig. 3). Surges and related hazards had not been previously highlighted in reports, although these pyroclastic currents can be deadly when they decouple from block-and-ash flows on steep volcano flanks, e.g. at Merapi: (Bourdier and Abdurachman 2001), Soufriere Hills, Monserrat (Druitt and Kokelaar 2002), and Colima (Saucedo et al. 2004). On 29 December 2002, a wet ash deposit, singed trees, and some damage were identified over a distance of 0.5 to 1 km along the 5-km long right bank of the upper K. Bang valley on the SSE flank (GVN 2003; Figs. 3 and 6). This indicates that a wet pyroclastic surge swept across the forest and tilled land when the block-and-ash flows of a volume of 3.25×10^6 m^3 was channelled 11 km as far as the Supit borough of the town of Pronojiwo in the K. Bang valley (Figs. 1a, 3, and 6).

Superimposed on the two eruptive styles, the third style occasionally consists in lava flows erupting along >1-km long fissures on the cone's flanks (e.g. 1895 and 1941–1942 on the ESE flank: Table 1). The 1941–1942 lava flow blocked the upper course of K. Besuk Semut at 940 m asl., diverting its drainage toward the C. Lengkong River. Other lava flows of prehistoric age have formed a lobate topography on the SW, SE, and E flanks of Semeru between 800 and 1,200 m asl, such as the Totoganmalang lava flow just N of the 1895 lava flow (Fig. 3). Pre-historic and historic flank lava flows fed by vents along NW–SE and ENE–WSW trending fractures suggest that mafic andesite lava is being stored at high levels in the cone, from where it can be diverted toward lateral dikes and sills that parallel regional trending faults.

Lahars threat, behaviour, and sediment yields

The emphasis on lahars pursues four objectives: (1) to assess the areas prone to lahar hazards and risks based on reports (Table 2) and the interpretation of 1981 and 1990 aerial photographs and of 1996, 2001, and 2003 SPOT satellite scenes (Fig. 5); (2) to identify some physical characteristics based on the sedimentology of the lahar deposits (Table 3; Figs. 7 and 8); (3) to estimate hydrodynamic parameters such as flow velocity, discharge, and total volume (Figs. 9 and 10) based on the analysis of video-tape recordings of active lahars taken at the C. Lengkong station; and (4) to establish a sediment budget and track the geomorphic evolution of lahar-fed channels based on surveys of the C. Lengkong river channel (Table 4). Direct observations and measurements of active lahars have hardly been confronted to results found through analogical models of lahar behaviour using surveys (Pierson 1985), flumes (Iverson 2003; Major and Iverson 1999), hydraulic models (Berzi and Mambretti 2003; Itoh et al. 2003; Liu and Huang 2003), and mathematical models (Savage and Iverson 2003; Takahama et al. 2003; Ancey 2003). We therefore need to compute in situ hydraulic parameters of active lahar, which can help to calibrate lahar modelling.

Table 3 Hydraulic parameters and deposit characteristics of lahars in the C. Lengkong River in 2000 (and two events in 2002–2003 for the purpose of comparison)

Flow									Deposit			
Flow Type	Year: 2000 Date	Time occurrence at village	Velocity front ($m\ s^{-1}$)	Discharge at front ($m^3\ s^{-1}$)	Depth max–min (m)	Q peak discharge $m^3\ s^{-1}$	Lahar runoff $10^3\ m^3$	C max volume (%)	Deposit thickness (m)	Bed No. & thickness (m)	Sediment. rate ($cm\ min^{-1}$)	Vol. sed. ($10^3\ m^3$)
HF	17 Jan	09:55	4		1.5	51	119	38				20
DF	18 Jan	15:00	2.5–3	85	1.7–0.3	136 (85)	212	50	110	4–27.5	3.7	98
Sf	19 Jan	16:00	5		1	19	33	7				4
Sf	29 Jan	14:15	4		1	17	65	7				2
DF	4 Feb	16:00	5–6	120	1–0.5	100 (120)	382	39	66	2–33	1.3	134
HF	23 Feb	14:00	5–7.5	60	0.8–0.15	68 (90)	240	31	80	4–20	5.3	45
Sf	24 Feb	13:00	4		0.9	72	266	10				11
DF	25 Feb	13:00	2	94	2.5–0.45	175 (135)	708	60	207	6–35	4.6	354
DF	29 Feb	16:00	1.9–4		1	86	447	23				49
DF	8 Mar	15:00	3.8–4	75	1–0.4	100 (90)	400	44	84	4–21	2.1	105
Sf	9 Mar	13:05	1.9–2	19	2–1	200 (100)	783	23	152	5–30	1.5	139
DF	23 Mar	14:30	1–1.4	29	1.3–0.15	104 (117)	319	59	130	4–33	8.7	153
DF	24 Mar	13:30	2–2.3	162	3.5–0.2	245 (175)	739	62	184	7–26	9.2	402
DF	27 Mar	14:00	2–2.3	69	3.5–0.5	245 (175)	1041	53	200	6–33	4	502
DF	28 Mar	13:30	2	60	1.5	150 (135)	608	55	142	5–28	7.1	283
DF	9 Apr	12:15	3		1.5	120	482	58				245
DF	13 Apr	14:30	2		1	100	450	47				190
DF	14 Apr	12:00	3		0.9	85	311	41				108
DF	15 Apr	15:30	1		1.5	135	511	56				233
HF	16 Apr	12:00	2		1	90	362	35				70
Sf	17 Apr	14:30	5		1.5	135	522	3				12
HF	23 Apr	16:00	3		0.6	54	260	40				80
Sf	13 May	07:00	2		1	80	423	23				56
HF	22 May	15:50	5		2	200	741	42				243
DF	28 Jul	09:00	1.5–2	90	3–0.25	240 (150)	945	60	188	5–38	7.5	430
Sf	18 Oct	07:40	4		0.5	35	152	5				3
DF	13 Nov	15:10	3		3	180	790	64				444
DF	15 Nov	15:15	4		1	100	439	48				115
DF	19 Nov	14:20	3		3	210	798	61	61			429
DF	20 Nov	15:15	4–4.5	90	3.5–0.4	245 (280)	792	63	210	4–53	5.3	396
Sf	22 Nov	12:10	5		0.8	75	347	19				30
DF	23 Nov	12:25	4–4.3	86	1–0.25	90	332	37	100	4–25	4	88
DF	26 Nov	14:10	3	150	2.7–0.25	180	872	64	300	4–75	12	499
Total							15.89	40				5.97
Mean			3		2	127	493	64				186
Maxi			5		3	245	1041	3				502
Mini			1		1	17	33	40				2

DF	19 Jan 2002	13:58 (90 min)	Max 6.7		4.5	571	452		186
HF	23 Jan 2003	11:01 (>90 min)	3.2 max 6		1.4	222	644		199

Key: Time of occurrence at C. Lengkong village; velocity of lahar front, in m s^{-1}; maximum and minimum lahar depth, in meter; Q peak discharge, in m^3 s^{-1}; runoff during the first 100 min of flow; Vs: volume of deposit during the first 100 min of flow; *Cmax* Maximum sediment concentration per volume within flow following front; Flow type: DF Debris flow, *Hf* Hyperconcentrated flow, *Sf* streamflow; Lahar deposit thickness, in m.; Average number and thickness of beds; Minimum sedimentation rate, in cm min^{-1}; *Vol. sed.* volume of sediments $\times 10^3$ m^3 (see Lavigne and Suwa 2004)

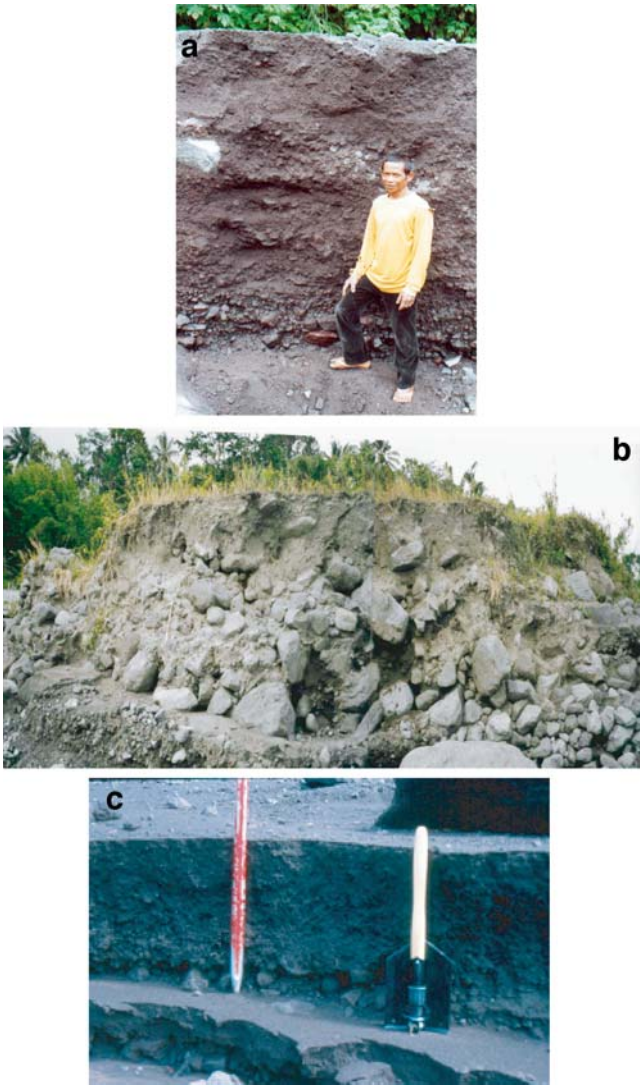

Fig. 7 Facies of the three principal lahar deposits: **a** a matrix-supported debris-flow deposit in 2003 (1.5-m tall boy as scale), Lengkong River, 1 km upstream of station; **b** historical (1909?) non-cohesive clast-supported debris-flow deposit (ice axe is 1 m long), Besuk Sat River, 11 km away from summit; **c** a hyperconcentrated streamflow deposit in 2003 (shovel is 0.5 m long), Lengkong River 9.5 km away from summit near station

Assessment of lahar-prone areas

An area of about 350 km^2 of channels and low terraces can be flooded by lahars on the Semeru's ring plain, which is larger than that threatened by lahars around Merapi (Thouret et al. 2000). Semeru's lahars can travel runout distances 15 to 35 km as debris flows onto the ring plain below 600 m asl (Fig. 2). Excess runout is due to: (1) high gradient rivers (27%) draining the E, SE, and S flanks; (2) gentle slopes (0.6 to 0.2%) in the ring plain that extend 25 km S and SE and >35 km E of the volcano; and (3) overbank and avulsion processes along wide, braided channels that do not deeply cut into subdued terraces; and

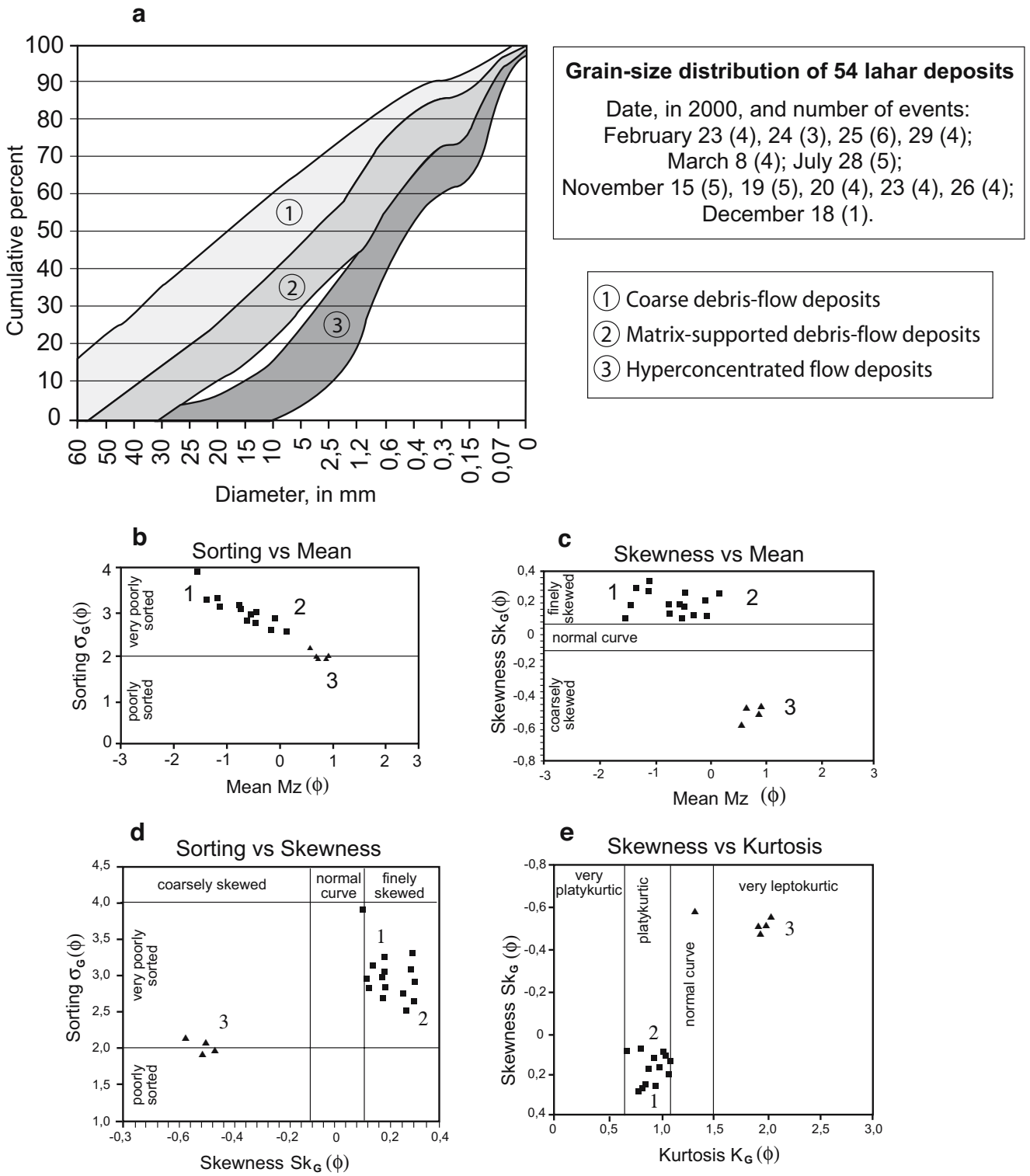

Fig. 8 **a** Grain-size distribution curves of 54 lahar deposits (February, March, and November 2000) in the C. Lengkong River. Grain-size parameters: **b** Sorting vs Mean index; **c** Skewness vs Mean; **d** Sorting vs Skewness; **e** Skewness vs Kurtosis, showing two principal and a subordinate categories of deposits

(4) several abandoned drainages that can be used by lahars further E and SE on the ring plain.

Rain-triggered lahars permanently threaten the densely populated ring plain, as shown by dark or bluish green lahar deposits in all drainages on SPOT images (e.g. Fig. 5). As much as 2,000 to 3,700 mm of rain fall per year on the E and SE Semeru's flanks and 200 mm of rain can fall in 24 h every 5 years on average (Siswowidjoyo et al. 1997). As a

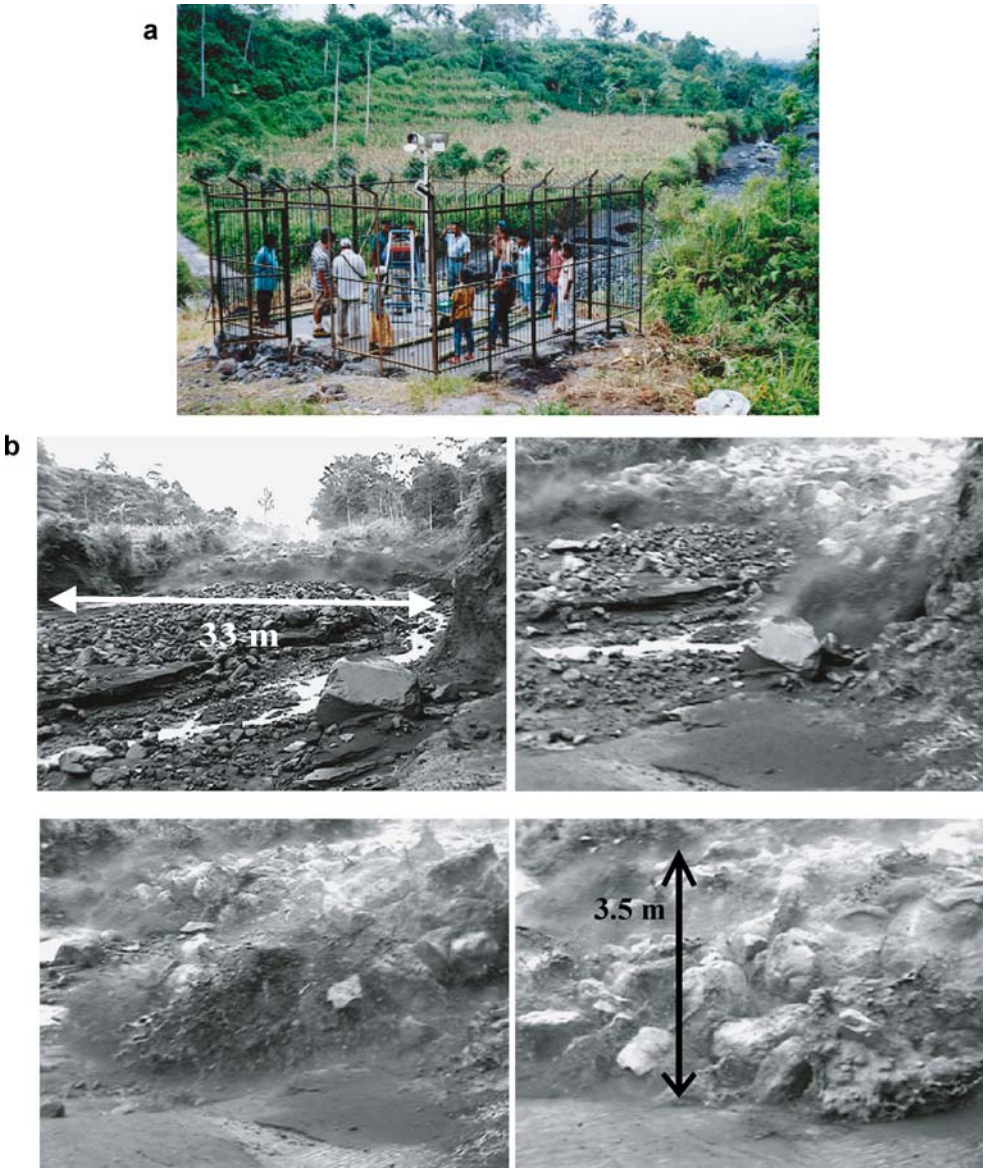

Fig. 9 **a** Fixed video camera at the station at 740 m asl in the C. Lengkong River 9.5 km ESE of the crater (located in Figs. 1 and 5). **b** Four video-tape frames recorded by F. Lavigne, looking WNW upstream channel on 19 January 2002: motion and front of a non-cohesive clast-supported debris flow (peak discharge 490 m^3 s^{-1}) advancing at a velocity of 5.7 m s^{-1} towards the observer located near the Curah Lengkong station

result, tens of lahars, commonly hyperconcentrated flows, are conveyed each year through the Koboan–Lengkong valleys toward the Rejali River or through the Kembar–Bang valleys toward the Glidik River (Figs. 2 and 3), which are building volcaniclastic deltas on the seashore almost 30 km away from the summit.

Table 2 displays lahar magnitude and recurrence: small-scale lahars (Q<400 m^3 s^{-1} and V<100,000 m^3) several times each season, medium-scale lahars (400<Q<600 m^3 s^{-1} and 100,000–1,500,000 m^3) at least once a year, and large-scale lahars (Q>600 m^3 s^{-1} and V 1.5–6 million m^3) every 6 years on average. Voluminous debris flows triggered by landslides combined with heavy rainfall exceeded 6 million m^3 in 1909 and 1981 on the E flank (Siswowidjoyo et al. 1997). A few hours before the large-scale 14 May 1981 debris flows, the now abandoned Tawonsongo observatory (left bank of Besuk Sat at 800 m asl) recorded about 300 mm of rain in 3 h.

Following past disasters, people have left the Lumajang district after the 1976 and 1981 disasters and have done so at least until 1999 although control countermeasures have been undertaken. Following the 1909 disaster, 45 *gumuk pelarian* (artificial hills for escape) were erected by the Dutch colonial authorities 2–3 m above the gently sloping ground of the Rejali River basin and K. Tunggeng in the densely populated subdistricts of Candipuro and Pasirian (Suryo 1986). However they are now far too small to cope with the increase in population over the past 97 years. A warning system depending on the DVGHM-owned Observatory ‘Pos Gunung Sawur’ was established in 1953 (Figs. 2 and 5) but only one seismometer is operating except during crises (e.g. Dec. 2002–Jan. 2003). Two small

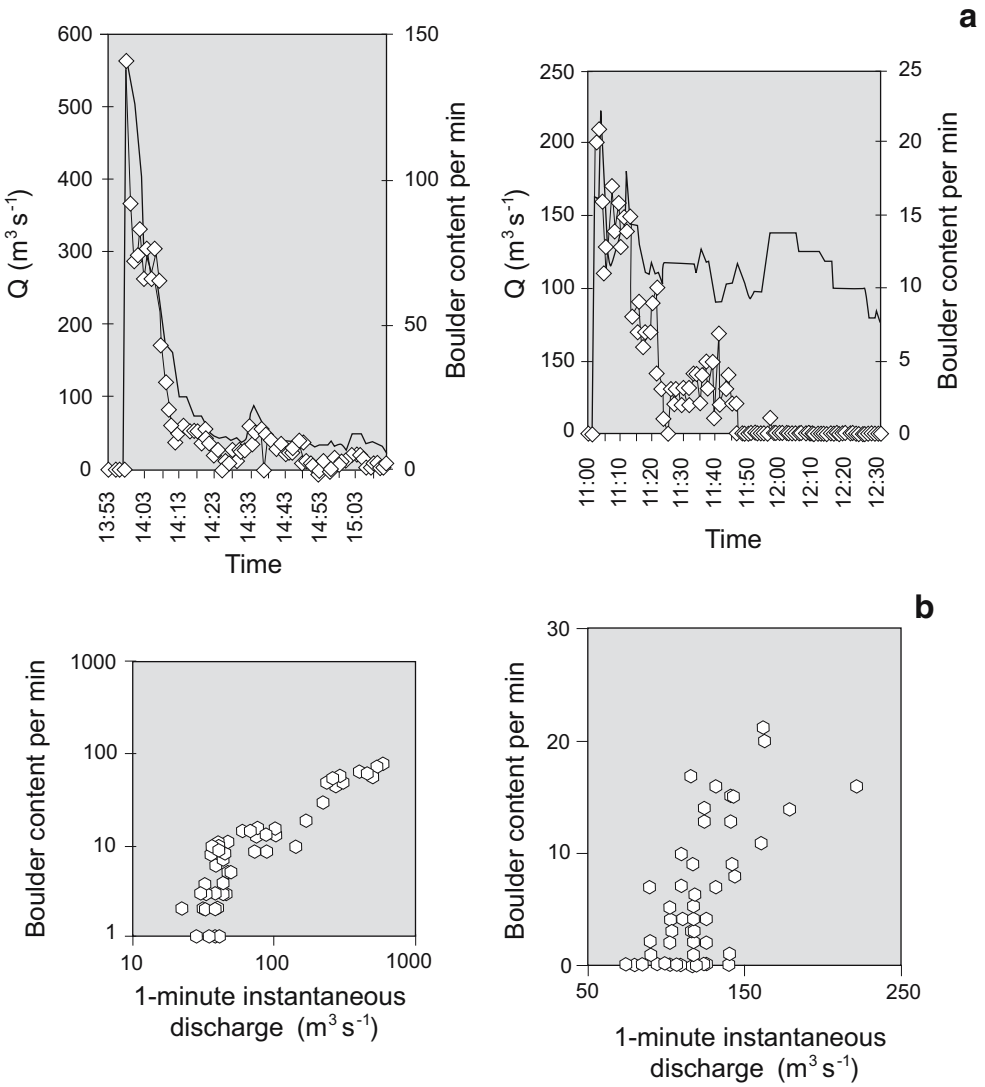

Fig. 10 **a** Variations in discharge (*black curves*) and large (>0.5 m) boulder flux per minute (*open diamonds*) based on video analysis (Lavigne et al. 2003) at the C. Lengkong station: *a* non-cohesive debris flow of 19 January 2002; *b* hyperconcentrated flow of 23 January 2002. **b** Correlation between discharge and large (>0.5 m) boulder flux per minute: *a* non-cohesive debris flow of 19 January 2002; *b* hyperconcentrated flow of 23 January 2002. In the case of hyperconcentrated flows (*upper right plot*), correlation between boulder content and instantaneous discharge is good during the first 15 min of the flow during which the sedimentation concentration is high (although there was no boulder- rich front). During the following 30 min, the poor correlation is due to the decrease in boulder content that the flows cannot transport. At the end of the flow, the diluted flow cannot carry 50 cm-sized boulders. For the purpose of comparison, debris flows show a very good correlation between the boulder content (measured through the section each minute), and discharge. The sediment concentration may not fluctuate much during the flow while it is not dilute. A fair amount of boulders stored in channel are readily available as they are stripped from previous lahar deposits, from the banks, and from the lava flow forming the river banks upstream of the station

observation posts at Tawonsongo (NE) and Argosuko (S) are abandoned. Projects on debris control (Sabo dams) have been carried out since the 1960s along the Koboan, Lengkong, and Rejali Rivers in the SE area, along the Besuk Sat and Tunggeng drainages to the E after the 1909 disaster, as well as in the valleys on the south flank (Yachiyo Engineering et al. 1986; Suryo 1986; Volcanic Sabo Technical Center VSTC 1989; Siswowidjoyo et al. 1997). In April 1977, the Semeru Proyek facility was created in Lumajang after the disastrous lahars of November 1976 (Table 1). Although Sabo constructions and repaired bridges represent an investment of several tens million US dollars in the Semeru ring plain, many inspected in the field are now filled up or damaged, and only half of the required number were constructed.

Physical characteristics of lahar deposits

Three categories of lahar deposits exist at Semeru (Fig. 7), comprising two end members, i.e. coarse clast-supported

debris-flow deposit and hyperconcentrated flow deposit, and an intermediate member, i.e. matrix-supported debris flow deposit. The field-based facies distinction is supported by grain-size distribution and granulometric parameters (graphic mean, sorting index, skewness, and kurtosis: Fig. 8), which help to distinguish hyperconcentrated flow deposits from non-cohesive, clast or matrix-supported debris-flow deposits. The three lahar groups display the following characteristics. Deposits of debris flows form a 2–3 m-thick bed in the current channel and a stratigraphic succession of alternating coarse and matrix-poor or matrix-rich beds. In contrast, ungraded deposits of hyperconcentrated flows form <0.5-m thick beds of coarse sand on the braided channel bottom and clast poor facies, and few gravel with virtually no clay and a scarce amount of silt. The facies of a debris-flow deposit is twofold: coarse, poorly sorted, clast-supported and non cohesive beds are much more abundant than matrix-supported and cohesive beds with a sole layer (Scott et al. 1995). The deposit is made up of gravel, cobbles, and boulders, coarse and fine sand, and a little amount of clay and silt (Fig. 8a).

Three types of small clasts (dense juvenile, vesiculated and juvenile, and weathered clasts) totalling about 5,000 grains 2.5–5 mm across were distinguished in order to determine the origin of transported sediments in 48 lahar beds (Gomez 2001). All deposits are rich in semi-vesiculated lava and scoriaceous lava or tephra (at least 70%), representing juvenile material remobilised from tephra-fall and pyroclastic-flow deposits. Oxidised lithic (non-juvenile) clasts represent ≥18%, while dense lava clasts make up ≤11% of typical lahar deposit. Componentry therefore suggests that the primary source for lahars is the juvenile tephra shed by Semeru and that bulking by incorporation of non-juvenile deposits along channels is probably limited except from other juvenile-sourced lahar deposits. Based on grain-size distribution and granulometric parameters, lahars display complex physical characteristics at Semeru. The majority (80%) of lahar events at C. Lengkong are hyperconcentrated flows, which do not derive from debris flows. They are controlled by entrainment of material from the channel bed. Debris flows (20% of events) are primarily driven by two regimes that may coexist in distinct parts of the turbulent flow with a vertically homogeneous distribution of the concentration: a collisional–frictional regime at the cobble-rich, matrix-depleted front and a frictional–viscous regime of the fluidised flow body (Iverson 1997). The hyperconcentrated flows reach the plain or the seashore without transforming to streamflow. During a lahar event at the Lengkong station (typically 90 to 120 min), the fluctuations of the measured sediment concentration vary from a prevailing regime of hyperconcentrated streamflow to a debris flow regime.

Hydrodynamic characteristics of lahars

A detailed study of active rain-triggered lahars has been carried out in the Curah Lengkong valley, a 10-km long tributary to the Koboan River on the SE flank. The

Table 4 Comparison of sediment discharge and hydro-geomorphological characteristics at active composite cones

Volcanoes and drainages	Yakedake[a] Kamikamihori R.	Unzen[b] Mizunashi R.	Merapi[3c] Bebeng R.	Semeru[d] C. Lengkong R.
Parameters				
Summit elevation (m)	2,445	1,473	2,911	3,676
Relative height (m) between Summit and observation site	865	1,392	2,100	2,800
Full length of the stream (m)	2,500	7,500	14,000	10,000
Mean stream gradient (%)	20.7	10.9	9.9	18
Slope angle at the observation station (%)	7	2.7	2.8	8.8
Catchment area for the observation site (km^2)	0.83	12	5	25.8
Mean annual precipitation (mm)	2,600	3,100	4,500	3,700
Time after last effective eruption (year: eruption year)	33 (1962)	0 (1991–1994)	11 (1984)	0–3 (1995–2002)
Permeability at the surface (cm s^{-1})	10^{-2}–10^{-3}	10^{-3}–10^{-5}	10^{-2}–10^{-3}	10^{-2}–10^{-3}
Frequency of debris flow (per year)	0.7	23	5	>10
Total bulk volume of transported sediment (10^4 m^3 $year^{-1}$)	0.5	210	20	700
Specific sediment transportation 10^4 m^3 km^{-2} $year^{-1}$	0.6	17.5	4	27
Annual depth of sediment yield (mm per year)	6	17.5	40	270
Average annual sediment yield (10^4 m^3 km^{-2} yr^{-1}) over 1–3 years	4 (3 years)	15 (3 years)	27.5 (3 years)	27 (1 years)

[a, b] Suwa and Yamakoshi 1999
[c] Suwa and Sumaryono 1996; Lavigne 2004
[c, d] Lavigne and Thouret 2002a, b; Thouret 2004

catchment has a drainage area of 25.8 km^2 and an average gradient of 18% (Fig. 6). The narrow and rectilinear C. Lengkong channel is not adjusted to actual streamflow processes. The 1941 lava flow shifted the Besuk Semut drainage toward SW, which has benefited to the previously small stream of C. Lengkong. Although the piracy has enhanced downcutting and lateral bank erosion at the edge of the lava flow since 1942, the straight C. Lengkong profile has not been adjusted yet to the change in catchment surface area. The platform of a video-camera station was constructed in January 2003 by the Mt. Semeru Project (Lumajang) on the left bank, 11.5 km downstream of the vent at an altitude of 750 m asl (Fig. 9a), and the video camera triggered by an upstream geophone (vibration sensor) was provided by H. Suwa (Kyoto University). The observation site fulfils four criteria: (1) tens of lahars occur per year in the valley, whose catchment covers Semeru's wettest flank (Siswowidjoyo et al. 1997); (2) a 30-m wide and rectangular channel enables in-situ measurements of velocity, discharge, and sediment concentration; and (3) a gravel road allows a prompt evacuation in case of a voluminous lahar. In addition, an automatic rain gauge was installed in 2003 in the Lengkong catchment at G. Leker (Fig. 2), 6 km from the summit at about 1,330 m asl, where > 2,700 mm of rain fall per year.

Measurements of active lahars have enabled us to estimate several hydraulic parameters in the C. Lengkong River (Table 3; Lavigne and Suwa 2004), including lahar volume and sediment flux. The concentration of sand and pebbles was calculated through direct sampling using buckets tossed into the flow. The content of cobbles and boulders was estimated on the basis of visual observations and video-tape recordings (Lavigne et al. 2003). In 2000, the eight largest rain-induced lahars each transported a volume of 4–5.7×10^5 m^3 of sediment through the river. Each event emplaced four to six beds of hyperconcentrated-flow and matrix-supported debris-flow deposits totalling 0.8 to 3 m in thickness. With flux velocities of 1.5 to 7.5 m s^{-1}, hyperconcentrated flow discharges ranged between 85 and 280 m^3 s^{-1}, whereas the discharge of large-volume debris flows lay in the 300–500 m^3 s^{-1} range. At the station, about 8 km downstream of the area of flow initiation, the flow front velocity has decreased to 3 m s^{-1}, due to the declining channel gradient, to the moving "dam effect" and to the grain size of the bouldery front of the flow, whose pore pressure is low. By contrast, pore pressure and discharge of the flow body, almost liquefied, are higher than at the flow front. Behind the front, the flow becomes hyperconcentrated over a time period of 10 to 20 min.

The sedimentation rate (i.e. deposit thickness divided by the inferred period of deposition between the flow front and flow peak) represents only a minimum velocity if the peak flow has lasted for several tens of minutes. Real time observations of flows, combined with grain-size distribution of lahar deposits (Figs. 9 and 10), have allowed us to compute sedimentation rates of 1.3 to 12 cm per minute (Lavigne and Suwa 2004). Such rates are correlated with the sediment concentration of the lahars (R^2=0.74), which can be expressed by an exponential equation:

$$\mathrm{Vs} = 0.29e^{0.10C} \quad (1)$$

where Vs is the velocity (m s^{-1}) of deposition and C is the average sediment concentration (% in volume) in gravel- and sand-sized (<5 cm) sediments sampled in 16 lahars by means of buckets.

The next research step on lahar hydrodynamics aims to combine the analysis of flow motion based on video tape recordings with the lahar components. Video-tape recordings, as well as geophones or seismometers, have long been used as a warning system for detecting lahars (Suwa 1988; Suwa and Sumaryono 1996) but they also provide a tool for fundamental research (Lavigne and Thouret 2000). This method has sometimes been used for describing lahars (Pierson 1985) and for estimating the content of transported boulders (Suwa 1988; Suwa and Yamakoshi 1999; Ikeda and Hara 2003). Use of seismometers and geophones for detecting large boulders in lahars has been tested at Merapi (Lavigne et al. 2000a) and at Pinatubo (Tuñgol and Regalado 1996). Distribution of pore pressure, which is thought to be a key parameter in the debris flow regime

Table 5 Frequency, magnitude, travel distance and other parameters for hazardous events (pyroclastic density currents) at Semeru based on reports or records since 1885

Type of pyroclastic density currents	Gravity-driven dome avalanches 'guguran'	Channeled block-and-ash flows	Scoria-and-ash flows and ash-cloud surges	Undifferentiated pyroclastic flows or avalanches*
Average (year) recurrence	Every month to every year	3.5	4–5	Several per year
Volume (10^6 m^3)	0.001≤average≤0.01 each	1.5–7.5	3.5–6	1–3
Travel distance, in km	0.25–1.5	3–11	7–10	2.5–7

Undifferentiated: unrecognized type of density current and (or) reported "summit lava flows", i.e. avalanches of dome or extrusive lava at vent and at the scar headwall. Channelled pyroclastic flows are >1.5-km long and have a volume >0.1 million m^3

Table 6 Frequency, magnitude, travel distance and other parameters for hazardous events (tephra fallout from eruption columns) at Semeru based on reports or records since 1885

Time of occurrence	Dry season (June–September)	Wet season (October–May)
Height (above vent) and frequency	300- to 600-m high columns 40 to 90 times per 'normal' day; 0.95- to 3.3-km high several times every 1 to 6 months; 3- to 7.05-km high every 2 to 5 years during larger eruptions; 1998–2003: average column 2.45- to 3.95-km high	
Plume direction	WSW, SW, SE, SSE (S)	NW, NNW, SSW (SW)
Distance of ashfall dispersal	Average 20–40 km; maximum 100 km	Average 20 km; maximum 75 km
Average volume per year	40,000 m^3 (Siswowidjojo et al. 1994)	

(Iverson 1997) and deposition (Major and Iverson 1999), is controlled by the grain-size distribution and grading of transported material in lahars, as the largest boulders are pushed toward the flow top, front and margins. Although observed in natural and experimental channels (Iverson et al. 1992; Major and Iverson 1999), this process cannot be easily modelled owing to the lack of precise data on size and distribution of transported boulders as well as on the distribution of flow velocity and solid discharge. In particular, large boulders (>50 cm) can hardly be taken account of in laboratory experiments and in grain-size analyses.

Frame by frame analysis of video-tape records taken at the C. Lengkong observation site in January 2002 and by a fixed video camera since January 2003 (Fig. 10a) have allowed us to compute quasi real-time velocity, discharge, and sediment load during flow motion, and also boulder content at lahar front (Lavigne et al. 2003). On 19 January 2002, an unusually large lahar was recorded (Fig. 10b), triggered after a period of four days of rainfall totalling almost 400 mm (including 140 mm on 19 January 2002). The estimated frontal velocity was 5.7 m s^{-1} and the peak discharge 571 m^3 s^{-1}. Table 3 summarises a series of measured parameters (occurrence, duration, velocity, volume, sediment concentration, boulder content) of hyperconcentrated flows and debris flows at the station. These hydrodynamic parameters are correlated with variations in discharge induced by proportion of boulders either jumping or entrained as bedload on the channel bottom. A fair correlation (r=0.90) exists between the instantaneous (1 min) discharge and the content of large (>50 cm) boulders at the flow front (Fig. 10). Discharges of non-cohesive debris flows have been correlated with the number of transported boulders. In contrast, the correlation between discharge and a small amount of boulders in hyperconcentrated flows is low (Fig. 10; Lavigne et al. 2003).

Annual sediment transfer in the catchment of the C. Lengkong River

Situmorang (1989) and Siswowidjojo et al. (1994) estimated that half of the annual pyroclastic debris expelled by Semeru is transported by rain-triggered lahars, due to intense tropical storms during rainy seasons. Our study of sediment transfer at Semeru aims to: (1) compute the sediment yield in a drainage basin; (2) assess the origin of the transported material; and (3) compare the results with data obtained on similar lahar-producer volcanoes (Major et al. 2000). A DEM of the Lengkong catchment (25.8 km^2) has been computed and deposits mapped (Fig. 5) in order to estimate a sediment budget. This takes account of material being ejected from the vent onto the upper catchment on a daily basis and material being transported through the channels by runoff, gully erosion, lahars, and streamflow during the rain season and sometimes even during the 'dry' season (e.g. July 2000: Fig. 8).

Denudation rates in disturbed catchments at persistently active volcanoes are difficult to estimate with accuracy and therefore are scarce. Despite uncertainties due to difficulties in collecting data, the Semeru's sediment yield calculated in the C. Lengkong catchment (2.7×10^5 m^3 km^{-2} $year^{-1}$) is of the same order of magnitude as the one calculated in the aftermath of explosive eruptions of large magnitude (Table 4). Sediment yields on volcanic slopes in wet environments set world records (10^5–10^6 m^3 km^{-2} $year^{-1}$) (Major et al. 2000; Lavigne 2004). Although erosion rates can reflect dissection of different types of fresh deposits on active volcanoes, two case studies are distinct: (1) sediment yields usually peak during the first years following a large ignimbrite-forming eruption such as the June 1991 Mt. Pinatubo event (10^6 m^3 km^{-2} $year^{-1}$: Pierson et al. 1997) or a medium-sized eruption forming a debris avalanche such as the 18 May 1980 event at Mt. St. Helens (10^5 m^3 km^{-2} $year^{-1}$: Major et al. 2000); (2) high erosion rates of 10^4 to 10^5 m^3 km^{-2} $year^{-1}$, due to frequent lahars, characterise the persistently active composite cones, which erupt tephra fallout and block-and-ash flows under wet climate. Sakurajima (Hirano and Hikida 1985), Merapi (Lavigne et al. 2000a, b), and Semeru rank among Earth's greatest sediment producers at long time scales.

In the C. Lengkong catchment (25.8 km^2), erosion produced an annual loss of 7 10^6 m^3 of sediment, i.e. 2.7×10^5 m^3 km^{-2} in 2000 (Lavigne 2004). Based on analysis of 24 lahar bed deposits with a bulk density of

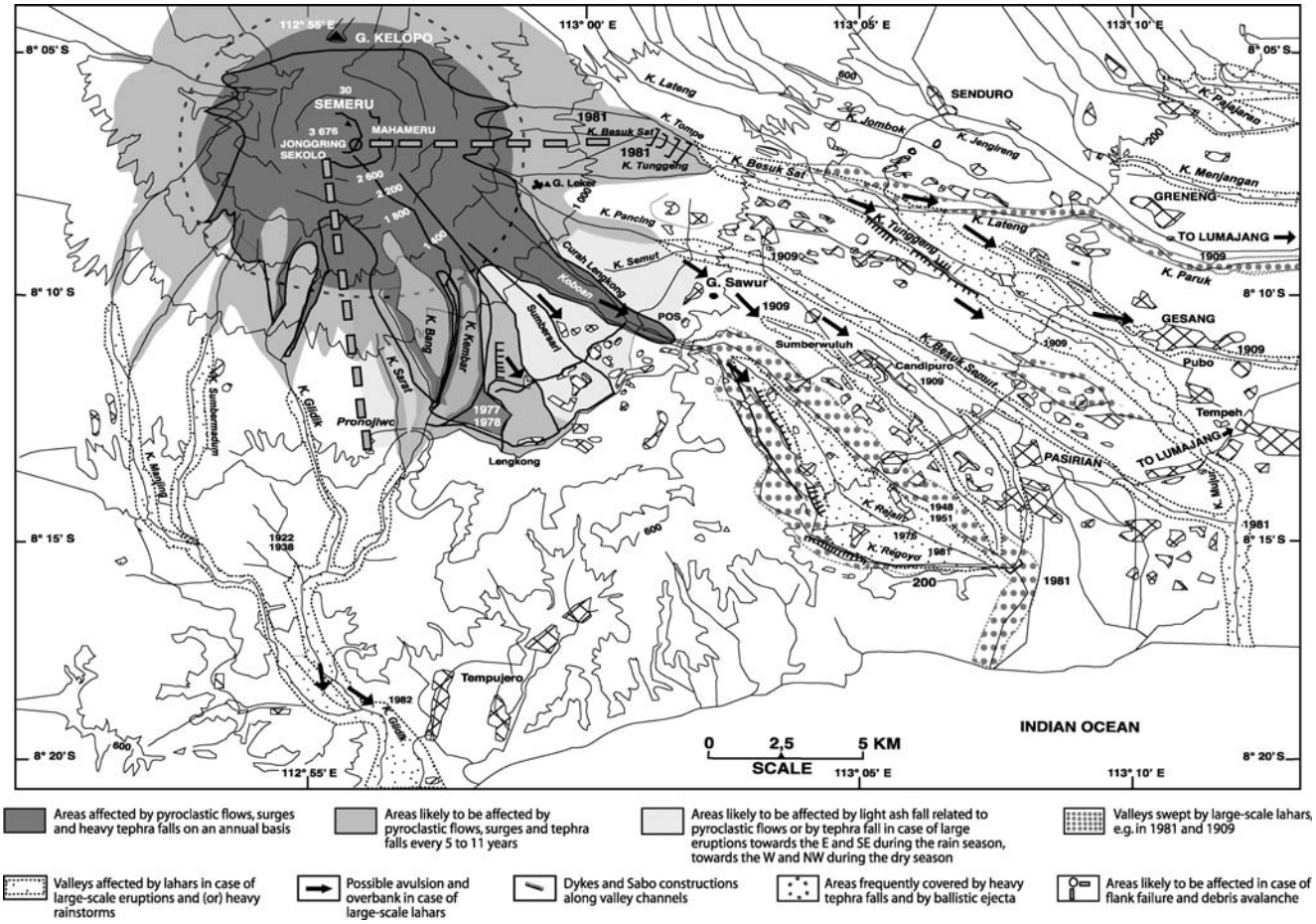

Fig. 11 Hazard-zone map of the proximal and medial Semeru's flanks depicting the extent of volcanic phenomena in the case of a probable medium-sized eruption scenario, based on the 1994, 1995, and 2002 eruptions and lahars. Distal areas: extent of lahars and floods in the case of a catastrophic eruption scenario and effects on the distal ring plain around Semeru, based on the 1909 and 1981 events and on the disaster-prone areas map (VSI, Bronto et al. 1996)

1,640 kg m^3 (owing to a scoriaceous texture), the average annual denudation rate is estimated at 4.4×10^5 t km^{-2} $year^{-1}$. Erosion acts as a fourfold process in the C. Lengkong channel: sheet and rill erosion, gully erosion, and undercutting of banks. Sheet and rill erosion removes ashfall deposit strewn by daily explosions, which yields a rate of 4×10^4 m^3 $year^{-1}$. Such remobilised ash is responsible for the amount (>18%, without comminution) of fine to medium-sized sand in lahar deposits (Fig. 8). Hyperconcentrated flows scour pyroclastic-flow deposits from river channels and banks. The contribution from this source is attested to by sandy–gravel or gravelly–sand textures, poor sorting, and bimodal grain-size distributions of the lahar deposits (Fig. 8). The banks of the C. Lengkong are undercut, a process which triggers landslips and rockfalls. Two categories of deposits are subsequently incorporated into lahars: (1) lava blocks >1 m in diameter, which fall from the 25-m high wall of the lava flow along the C. Lengkong between 1470 m and 870 m asl; (2) finer-grained and weathered debris from 'old' pyroclastic and lahar deposits. The latter source contributes for about 14% of lahar material based on the amount of oxidised scoriaceous material.

The high erosion rate at Semeru compares well with similar values estimated at other active composite cones in wet environment (Table 4). This is due to the constant generation of pyroclastic material in the summit area, which is remobilised by runoff during the rainy season and even during the 'dry' season. In Table 4, the highest rates have been calculated during the first years following a high magnitude (>volcanic explosivity index [VEI] 3) explosive eruption such as the 1991 Pinatubo event. As the return frequency of these eruptions exceeds 100 years on average, the denudation rate at the century scale is low. By contrast, denudation rates at Sakurakima, Merapi, and Semeru, which are induced by a steady supply of pyroclastic debris, can be considered as constant on an annual basis. Therefore, Semeru's denudation rate is, along with Sakurajima, arguably the highest on a volcano worldwide (Lavigne 2004).

Synthesis: hazard assessment and maps

The delineation of hazard-prone areas, now 600 km^2 (Fig. 1), stems from numerous reports on the Semeru's activity (Tables 1, 2, 5 and 6), which have been published by Dutch geologists since 1884, the Volcanological Survey of Indonesia since 1986, and the Smithsonian Institute (GVN Bulletin) since 1996. Semeru has erupted every 1.5 years while dormant periods have merely exceeded 2.7 years on average, although such periods have lasted 11 to 28 years before the 1941 lava flow eruption (Table 1). In contrast, no repose period has been reported since 1967.

Hazard assessment

Tables 2, 5 and 6 summarises the magnitude and frequency of lahars, pyroclastic flows, and tephra.

Lahars at Semeru caused >1000 casualties during the 20th century alone, devastating more than 40 villages and 110 km^2 of tilled land since 1884 (Table 1). Debris flows are even more deadly than pyroclastic flows at Semeru because they can occur in any year, even in the absence of an eruption. Small debris flows occur every three days on average during the rainy season between October and May, with sizeable lahars killing people and causing damage every 6 years on average since 1884 (Table 1), and large-volume debris flows bringing havoc to the Semeru's ring plain in 1909 and 1981 (Fig. 2). In addition, landslide-induced debris flows have occurred during periods of relative quiescence, in particular on the E flank drained by the Besuk Tengah and Tompe Rivers.

Based on the chronicles and reports since 1884, we distinguish three categories of flows (Table 5); small-volume gravity-driven rockslide avalanches ($<0.1\times10^6$ m^3) produced by dome extrusion and collapse; scoria-rich (and lithic-rich) pyroclastic flows of moderate volume ($0.5–3\times10^6$ m^3) and range (2–7 km); and large-volume block-and-ash flows (3 to 6×10^6 m^3, with or without pyroclastic surges) that can reach villages 12 km away from the summit. Compared to Merapi block-and ash flows, the exceptional excess runout of Semeru's pyroclastic flows is due to a relatively low H/L= 0.25 (0.33 at Merapi). The relatively low H/L ratio is related to an extensive ring plain (>35 km to the East) and to the collapse of small low-altitude columns (typically ≤3 km above the vent). The excess runout is also due to the fact that scoria and sand-rich flows are more mobile than the block-and-ash flows. Channelled pyroclastic flows can therefore travel farther through gorges into populated areas (e.g. Pronojiwo near the K. Bang River). Flows eventually expand onto fans where volcanic debris has accumulated against hill scarps running west to east (Fig. 2, e.g. Sumberurip and Supiturang near the Lengkong River, not the C. Lengkong). Figures 1, 2, 3, and 5 show the extent of the most widespread pyroclastic flows, debris flows, and lava flows of Holocene and historical age. The thick black line along K. Bang in Fig. 3 depicts the area affected by the voluminous 29 December 2002 pyroclastic flow (Purbawinata et al. 2003).

Tephra fall are usually light on the ring plain (a few millimeters 12 km SE of the vent on 29–30 December 2002) but can reach 5 centimeters at 950 m asl. on the SE flank during larger eruptions (1977–1978; Table 6). Tephra fall can be deadly within 3 km around the summit vent and meter-sized ballistic blocks are ejected >1 km away from the vent. Ballistics killed two tourists on 2 September 1997, and two volcanologists on 27 July 2000 wounding three more (GVN 1999, 2000, 2001). Photographs and SPOT images show tephra-fall deposits (cinder, lapilli and blocks up to 1.5 m across) several meters thick on the Mahameru summit and on two thirds of the Semeru's cone-shaped summit, unvegetated down to about 2,000 m asl. The steep S, SE, and E slopes of the summit cone are more often mantled by ash than the SW, W and N slopes, and are scoured by a dense gully network (Fig. 4). Tephra are remobilised by large gullies that scallop the landslide scars in the K. Besuk Sat, Tengah, and Tompe headvalleys (Figs. 2 and 3), which have delivered debris flows into the K. Tunggeng drainage toward the E. Landslides are not triggered by forest clearing as demonstrated by the 1981 mass movements under the evergreen forest high on the E and NE flanks of Semeru.

Hazard-zone map

One hazard-zone map is provided based on differing eruption magnitudes, field surveys and detailed historical records (Fig. 11). The proximal and medial areas are potentially affected by tephra-fall, pyroclastic flows and surges, and by lahars in case of medium-sized events with a 3.5-year return frequency (e.g. 1994, 1995, 2002; Tables 2, 5 and 6). The medial and distal areas are potentially affected by ash fallout, pyroclastic flows and surges, debris avalanches, and lahars in case of large eruptions with a 7-year return frequency (e.g. 1909, 1975–1977). Two hazard prone areas must be added to the disaster-prone areas map (Bronto et al. 1996): a quadrant open at 90° to SE and E, likely to be affected by debris avalanche in case of failure of the upper E flank of Semeru, and the Mujur River drainage network that is likely to be flooded by voluminous debris flows triggered by landslides, heavy rainfall, and possibly earthquakes.

The delineated lahar-prone areas in Fig. 11 is a basis for a GIS-based risk evaluation of people, infrastructures, and elements at risk on the most affected SE flank of Semeru, which can update the 1996 disaster-prone map and plan precise risk mitigation procedures. Staple activities, resources, and people vulnerability in and along the valleys that convey lahars have formed several information layers

overlain in the georeferenced frame of the GIS ILWIS (Morelière 2001).

Three areas are the most hazard-prone at Mt Semeru. Firstly, a triangle-shaped area opening at 45° toward the SE with a width of ~15 km at 12 km from the vent, which is frequently swept by avalanches and block-and-ash flows. At least 100,000 people live in the lower part of the triangle-shaped area (e.g. Pronjiwo, Supiturang, Sumberurip; Figs. 1 and 2). Gravity-driven avalanches, produced by the collapse of lava extrusion at the vent, travel 1.5–3 km down the scar open to the SE. Block-and-ash flows are induced by dome collapse while scoria-and-ash flows are triggered by vulcanian events in open system (once the pressure of extrusive magma has exceeded the lithostatic resistance of the lava dome). Secondly, the E, SE and S valleys are threatened each year by tens of small to moderate-sized rain-triggered lahars that may reach the sea 25 km away. Another group of at least 100,000 people live in this area, although less exposed to pyroclastic flows and tephra fall. Lahars usually do not generate floods in the E ring plain because they are confined by dikes and Sabo dams constructed after the 1909 disaster. Thirdly, the structural boundary shown in Fig. 5 can favour a flank collapse of the steep-sided cone-shaped summit toward the SSE in the event of a major eruption. The extruding dome and(or) the scar walls can fail and produce debris avalanches and debris flows. These can cause extensive damage on the lower flanks and ring plain over distances of 30–35 km if avulsion diverts debris from the main valleys into the catchments of the Mujur, K. Lateng, and K. Paruk rivers (Figs. 2, 3 and 11). This is the cultivated and densely populated ring plain of Semeru where almost 800,000 people live, including the 80,000 population of Lumajang.

We cannot preclude a catastrophic eruption even though spreading of pyroclastic flows and lahars during the past two centuries has been restricted to the S and E slopes of Semeru: the S and E crater rims are lower than the N and W rims, buttressed by the Mahameru summit. A large dome rising from the vent floor could overflow the SW and NE crater rims: extruding lava has reportedly overcome the height of the vent rim from 1972 to 1977. In case of increase in magma output and dome growth, avalanches and pyroclastic flows could spill over the SW and the NE flanks of the volcano (e.g. Soufrière Hills at Montserrat after September 1997: Druitt and Kokelaar 2002).

Conclusions

From this research report, five categories of conclusions can be drawn. Firstly, the composite Semeru cone results from the growth of two edifices. The E and SE flanks of the modern cone have experienced landslides, a process which is favoured by the weathered bedrock beneath the volcano toward the SE. Further instability is not precluded as the summit cone is hosted in a weak structure attributed to an earlier collapse, and is cut by an active horseshoe-shaped scar.

Secondly, the wealth of reports describing activity at Semeru since 1884 has enabled us to describe a threefold explosive regime: (1) short-lived columns from phreatic or steam explosions occur several times a day; (2) "cannon-like" explosions produce 1–3 km high vulcanian columns that disperse ash >25 km toward the E, SE, and W–SW; (3) phreatomagmatic explosions expel small volumes of non-juvenile lava fragments and bread-crust bombs. Vulcanian and phreatomagmatic explosions, producing cock-tailed ash-laden high columns, reflect magma–water interaction at the vent floor. The first three regimes coexist with relatively slow rates of lava extruding from a dome plug. Vesiculated lava and lighter scoriaceous blocks of mafic andesite, dragged from the incandescent extruding lava, imply degassing processes involving magmatic gas interacting with an aquifer at the conduit-vent host rock boundary (GVN 1997). This interaction can explain three observations: short-lived vulcanian columns that produce little amount of ash but propel bread-crust bombs, incandescent blocks stripped off the extruding lava at the vent bottom, and light porous lava of the dome plug. In contrast, the second eruptive style is linked to accelerated eruption rates every 5 to 7 years. Increase in output rate of more volatile-rich magma trigger 3–7-km high columns producing ballistic bombs to 3 km and ash fall 45 km downwind, and block-and-ash flows, induced by dome collapse sweep the SE scar and channelled 5 to 12 km downstream at a about 5-year interval. Superimposed on the two eruptive styles, the third occasionally consists in lava flows erupting along >1 km-long fractures on the cone's flanks (e.g. 1895 and 1941–1942).

Thirdly, we have combined in-situ measurements and video surveillance analysis to obtain some hydrodynamic lahar parameters. Despite approximations at the catchment scale and uncertainties in collecting sediment concentration samples from active flows, the combined approach yields a sediment flux of 2.7×10^5 m^3 km^{-2} year^{-1} and a denudation rate of 10^5 t km^{-2} year^{-1} at Semeru. This rate is comparable to other examples of active, lahar-producing composite cones in humid climates, but is also of the same order of magnitude as rates estimated in the aftermath of large-magnitude explosive eruptions. At Semeru, the efficient denudation is a consequence of the short return period of lahars, generated in turn by a steady supply of pyroclastic debris and monsoon rainfall, which produce a high rate of surface runoff on the unvegetated, steep-sided cone (e.g. Yamakoshi and Suwa 2000).

Fourthly, Semeru is one of the most effective producers of lahars on Earth. Hyperconcentrated flows are more frequent in Semeru drainages than large debris flows but the latter, including primary (hot) lahars, are not unusual

during and after pyroclastic flows. Six rationale explain the efficient and rapid transfer of debris from the summit toward the ring plain: (1) rainfall as high as 3,700 mm per year and rainstorms of 500 mm in 48 h; (2) steady supply of debris on the summit, readily removed in the active scar toward the SE or toward the landsliding area on the E flank; (3) fine-grained ashfall deposit, which favours the initiation of hyperconcentrated flows on the summit slopes; (4) high-gradient channels on the cone-shaped summit (33° angle slopes above 1,700 m asl); (5) low H/L (=0.25) and long runout of lahars on a widespread ring plain (>35 km below 600 m asl); and (65) overbank flow and avulsion from a dense drainage network on the gentle sloping plain, enhanced by dikes and dams that are not well maintained.

Fifthly, one map delineates proximal, medial, and distal hazard-prone areas. The most endangered areas are: (1) a triangle-shaped area open toward the SE of the crater, which is frequently swept by dome-collapse avalanches and pyroclastic flows; (2) the S and SE valleys that convey tens of rain-triggered lahars each year over a distance of 20 to 25 km to the sea, and less frequent debris flows induced by landslides, which can flow 35 km on the ring plain to the E; and (3) the steep-sided cone-shaped summit that can fail and produce debris avalanches and large volume debris flows toward the SE and E ring plain.

Acknowledgments This work was supported by the former 'Coordination de la Recherche Volcanologique' (OPGC) and the Laboratoire Magmas et Volcans (UMR 6524-CNRS) in Clermont-Ferrand, by the Laboratoire de géographie physique (UMR 8591-CNRS) in Meudon, and by the grant No.15404017 in aid of Japan Society of the Promotion of Science. We thank the Semeru Volcano Observatory of the Geological Institute of Indonesia in Gunung Sawur, Mr. Dodi and Darmono of the Mt. Semeru Project in Lumajang, and, as well as the people of the Curah Lengkong village and L. Thouret for field assistance. Unpublished research reports from BSc. students E. Keim, M. Morelière, J. Declercq, T. Boyer, and B. Caron, have provided useful data to our study. Reviews by J.L. Macías and G. Carrasco-Nuñez have been appreciated. This is contribution No.5 of the ACI research programme 'Aléas et changements globaux' funded by INSU-CNRS.

References

Ancey C (2003) Role of particle network in concentrated mud suspensions. In: Rickenman D, Chen CL (eds) Debris-flow hazards mitigation: mechanics, prediction, and assessment, vol 1. Millpress, Rotterdam, pp 257–268

Berzi D, Mambretti S (2003) Mathematical modeling and experimental tests of unsteady flow of non-Newtonian fluids. In: Rickenman D, Chen CL (eds) Debris-flow hazards mitigation: mechanics, prediction, and assessment, vol 1. Millpress, Rotterdam, pp 447–456

Bourdier J-L, Abdurachman EK (2001) Decoupling of small-volume pyroclastic flows and related hazards at Merapi volcano, Indonesia. Bull Volcanol 63:309–325

Bronto S, Hamidi S, Martono A (1996) Disaster-prone zone map of Semeru volcano, East Java (1:50,000 scale). Direktorat Vulkanologi, Volc Survey Indonesia, Bandung

Carn SA (1999) Application of synthetic aperture radar (SAR) imagery to volcano mapping in the humid tropics: a case study in East Java, Indonesia. Bull Volcanol 61:92–105

Dana IN (1997) Perubahan morfologi Kawasan puncak dan pengaruhnya terhadap daeraah bahaya gunungapi, kasus G. Semeru (morphological changes of volcano summit and implication for volcanic hazards, Mt. Semeru as a case). Internal report, VSI, Bandung, pp 8

Dana IN, Wildan A, Agus Martono, Dio Sutresna, Triyono, Rochman, Djuadi (1996) Evaluasi kegiatan G. Semeru, Jawa Timur, Mei (assessment of the Mt. Semeru volcanic activity, East Java). VSI, Bandung, pp 44

Druitt TH, Kokelaar BP (eds) (2002) The eruption of Soufrière Hills volcano, Monserrat, from 1995 to 1999. Geol Soc London Mem 21:575

Gomez C (2001) Les lahars du volcan Semeru : dynamique et action morphogénique. (unpubl.) MSc report, université Paris I Panthéon-Sorbonne, pp 111

GVN (1996) Global Volcan Network Bulletin, Semeru 21(9):6, 21(11):9

GVN (1997) Global Volcan Network Bulletin, Semeru 20 (5):4–5, 22 (6):7, (8):2, (10):2

GVN (1999) Global Volcan Network Bulletin, Semeru 24(5):7, (8):6, (9):16

GVN (2000) Global Volcan Network Bulletin, Semeru 25(7):4–7

GVN (2001) Global Volcan Network Bulletin, Semeru 26(8):4–6

GVN (2002) Global Volcan Network Bulletin, Semeru 27(6):2, (9):7–8, (12):7

GVN (2003) Global Volcan Network Bulletin, Semeru 28(4):11–13, 28 (7):5, (9):7–8

Hirano M, Hikida M (1985) The distribution of volcanic ash around Mt. Sakurajima. In: Proceedings of the International Symposium on Erosion, Debris flows, and Disaster Prevention. Tsukuba, Japan, 3–5 September 1984, pp 261–264

Ikeda A, Hara Y (2003) Flow properties of debris flows on the Kitamata valley of the Name River, Japan. In: Rickenman D, Chen CL (eds) Debris-flow hazards mitigation: mechanics, prediction, and assessment, vol 2. Millpress, Rotterdam, pp 863–870

Itoh T, Miyamoto K, Egashira S (2003) Numerical simulations of debris flow over erodible bed. In: Rickenman D, Chen CL (eds) Debris-flow hazards mitigation: mechanics, prediction, and assessment, vol 1. Millpress, Rotterdam, pp 457–468

Iverson RM (1997) The physics of debris flows. Rev Geophys 35:245–296

Iverson RM (2003) The debris-flow rheology myth. In: Rickenman D, Chen CL (eds) Debris flow hazards mitigation: mechanics, prediction, and assessment, vol 2. Millpress, Rotterdam, pp 303–314

Iverson RM, Costa JE, LaHusen R (1992) Debris-flow flume at H.J. Andrews Experimental Forest, Oregon. US Geol Surv Open-File Report, pp 92–483

Kemmerling GLL (1922) Het Aquatische transport der Semeruproducten naar de omliggende vlakten (Het natte gevaar) (translated by K. Kusumadinata, 26 October, 1987). Vulkanol Meded 4:11–19

Kusumadinata K (1979) Semeru. Data dasar gunungapi Indonesia (Catalogue of references on Indonesian volcanoes with historical eruptions), VSI, Bandung, pp 304–320

Lavigne F (2004) Rate of sediment yield following small-scale volcanic eruptions: a quantitative assessment at the Merapi and Semeru stratovolcanoes, Java, Indonesia. Earth Surf Landf Proc 29:1045–1058

Lavigne F, Suwa H (2004) Contrasts between debris flows, hyperconcentrated flows and stream flows at a channel of Mount Semeru, East Java, Indonesia. Geomorphology 61:45–58

Lavigne F, Thouret J-C (2000) Les lahars: dépôts, origines et dynamique. Bull Soc Geol Fr 1741:545–557

Lavigne F, Thouret J-C (2002a) Erosion, sedimentation et lahars sur le volcan Semeru, Java est, Indonesia. In: Delahaye D, Maquaire O (eds) Geomorphology: from expert opinion to modelling. Université L Pasteur Strasbourg, 26–27 April 2002, pp 193–202

Lavigne F, Thouret J-C (2002b) Sediment transportation and deposition by rain-triggered lahars at Merapi volcano, central Java, Indonesia. Geomorphology 49:45–69

Lavigne F, Thouret J-C, Voight B, Young K, LaHusen R, Marso J, Suwa H, Sumaryono A, Sayudi DS, Dejean M (2000a) Instrumental lahar monitoring at Merapi volcano, Central Java, Indonesia. In: Voight B, Sukhyar R, Wirakusumah AD (eds) Merapi Volcano. J Volcanol Geotherm Res 100:457–478

Lavigne F, Thouret J-C, Voight B, Suwa H, Sumaryono A (2000b) Lahars at Merapi volcano, Central Java: an overview. In: Voight B, Sukhyar R, Wirakusumah AD (eds) Merapi Volcano. J Volcanol Geotherm Res 100:423–456

Lavigne F, Tirel A, Le Floch D, Veyrat-Charvillon S (2003) A real-time assessment of lahar dynamics and sediment load based on video-camera recording at Semeru volcano, Indonesia. In: Rickenman D, Chen CL (eds) Debris flow hazards mitigation: mechanics, prediction, and assessment, vol 2. Millpress, Rotterdam, pp 871–882

Liu KF, Huang MC (2003) Three-dimensional numerical simulation of debris flows and its applications. In: Rickenman, Chen CL (eds) Debris-flow hazards mitigation: mechanics, prediction, and assessment, vol 1. Millpress, Rotterdam, pp 469–480

Major JJ, Iverson RM (1999) Debris-flow deposition-effects of pore-fluid pressure and friction concentrated at flow margins. Geol Soc Amer Bull 111:1424–1434

Major JJ, Pierson TC, Dinehart RL, Costa JE (2000) Sediment yield following severe volcanic disturbance—a two-decades perspective from Mount St. Helens. Geology 28:819–822

Morelière M (2001) Les risques volcaniques : menaces, vulnérabilité, le volcan Semeru, Indonésie. (Unpubl.) MS report, université Lumière Lyon 2, pp 186

Mulyadi E (1992) Le complexe de Bromo-Tengger, Est Java, Indonésie. Etude structurale et volcanologique. (Unpubl.) PhD thesis, département de géologie, université Blaise Pascal, Clermont-Ferrand, pp 136

Nus-CRISP (2006) Images from space, Calendar 2006, ©Spot Asia, Centre for Remote Imaging, Sensing and Processing, National University of Singapore, Singapore

Pierson TC (1985) Initiation and flow behavior of the 1980 Pine Creek and Muddy River lahars, Mount St. Helens, Washington. Geol Soc Amer Bull 96:1056–1069

Pierson TC, Daag AS, Delos Reyes PJ, Regalado TM, Solidum RU, Tubinosa BS (1997) Flow and deposition of post-eruption hot lahars on the east side of Mount Pinatubo, July–October 1991. In: Newhall CG, Punongbayan RS (eds) Fire and Mud: eruptions and lahars of Mount Pinatubo, Philippines. University of Washington, Seattle, pp 921–950

Purbawinata MA, Hendrasto M, Martono A, Triastuty H, Rosadi U, Mulyana I, Suparno, Liswanto, Susanto (2003) "Hot News" Gunungapi Semeru, Kegiatan Awan Panas Desember 2002–Januari 2003. (Internal report on the Semeru pyroclastic flows, unpubl), VSI, G. Sawur, 4 January 2003, pp 7

Sadjiman, Iman K Sinulingga, Hendra Gunawan (1995) Penyebaran dan perhitungan volume awanpanas guguran G. Semeru, Jawa Timur, 20 Juli 1995 (Dispersion and volume calculation of dome-collapse pyroclastic flow at Mt. Semeru, East Java, 20 July 1995). VSI, Bandung, pp 14

Saucedo R, Macías JL, Bursik M (2004) Pyroclastic flows deposits of the 1991 eruption of Volcán de Colima, Mexico. Bull Volcanol 66:291–306

Savage SB, Iverson RM (2003) Surge dynamics coupled to pore-pressure evolution in debris flows. In: Rickenman D, Chen CL (eds) Debris flow hazards mitigation: mechanics, prediction, and assessment, vol 1. Millpress, Rotterdam, pp 503–514

Scott K, Vallance JW, Pringle PT (1995) Sedimentology, behavior, and hazards of debris flows at Mount Rainier, Washington. US Geol Surv Prof Paper 1547, pp 56

Simkin T, Siebert L (1994) Volcanoes of the world, 2nd edn. Smithsonian Institution, Geoscience Press, Tucson, Arizona, pp 349

Siswowidjojo S, Widaningsih N, Rubiati A, Mulyati B, De Neve GA (1994) Laporan pelaksanaan bimbingan gunungapi G. Semeru di Kabupaten Lumajang, Propinsi Jawa Timur, September 1994 (Report on works carried out at Semeru volcano in the Lumajang district, East-Java province, September 1994). VSI, Bandung, p 38

Siswowidjoyo S, Sudarsono U, Wirakusumah AD (1997) The threat of hazards in the Semeru volcano region in East Java, Indonesia. J Asian Earth Sci 15:185–194

Situmorang T (1989) Lahar and pyroclastic flow hazards zoning of Semeru volcano, East Java, Indonesia (using aerial photograph). International Symposium on Erosion and Volcanic Debris Flow Technology, Yogyakarta, Indonesia, July–August 1989, pp 12

Suryo I (1986) G. Semeru. Berita Berkala Vulkanologi. Edisi Khusus no. 111, VSI, Bandung pp 52

Sutawidjaja IS, Wahyudin D, Kusdinar E (1996) Geological map of Semeru volcano, East Java (1:50,000 scale). Direktorat Vulkanologi, VSI, Bandung

Suwa H (1988) Focusing mechanism of large boulders to a debris flow front. Trans Jpn Geomorphol Union 9:151–178

Suwa H, Sumaryono A (1996) Sediment discharge by storm runoff from a creek on Mount Merapi. J Jpn Soc Eros Control Eng 48:117–128

Suwa H, Yamakoshi T (1999) Sediment discharge by storm runoff at volcanic torrents affected by eruption. Z Geomorphol Suppl Bd 114:63–88

Takahama J, Fujita Y, Hachiya K, Yoshino K (2003) Application of two-layer simulation model for unifying debris flow and sediment sheet flow and its improvement. In: Rickenman D, Chen CL (eds) Debris-flow hazards mitigation: mechanics, prediction, and assessment, vol 1. Millpress, Rotterdam, pp 515–526

Thouret J-C (2004) Geomorphic processes and hazards on volcanic mountains. In: Owens Ph, Slaymaker O (eds) Mountain geomorphology, chapter 11. Arnold, London, pp 242–273

Thouret J-C, Lavigne F, Kelfoun K, Bronto S (2000) Toward a revised assessment of volcanic hazards at Merapi, Central Java. In: Voight B, Sukhyar R, Wirakusumah AD (eds) Merapi Volcano. J Volcanol Geotherm Res 100:479–502

Tuñgol NM, Regalado MTM (1996) Rainfall, acoustic flow monitor records, and observed lahars of the Sacobia River in 1992. In: Newhall CG, Punongbayan RS (eds) Fire and Mud. University of Washington, Seattle, pp 1023–1032

Van Bemmelen RW (1942) De Semoroe. Open File, Direktorat Volkanologi, VSI, Bandung (in Dutch), pp 12

Van Bemmelen RW (1949) The geology of Indonesia and adjacent archipelago. Government Printing Office, The Hague, pp 150

Van Padang NM (1951) Semeru. Catalogue of the active volcanoes of the world including solfatara fields. Part 1. Indonesia. Internat Volcanol Assoc, Napoli, Italy, pp 271

Volcanic Sabo Technical Center VSTC (1989) Geographical notes for volcanic debris control projects. Ministry of Public Works, Yogyakarta, pp 49–64

Wahyudin D (1991) Volcanology and petrology of Mt. Semeru volcanic complex, East Java, Indonesia. Diploma of Applied Science (Volcanology), Victoria University of Wellington, New Zealand, pp 126

Yachiyo Engineering, Nippon Koei, PT Tricon Jaya (1986) Engineering services on Mt Semeru urgent rehabilitation project. Detailed design main report, Bandung, pp 30

Yamakoshi T, Suwa H (2000) Post-eruption characteristics of surface runoff and sediment discharge on the slopes of pyroclastic-flow deposits, Mount Unzen Japan. Trans Jpn Geomorph Union 21:469–497